

International Journal on

Advances in Telecommunications



2016 vol. 9 nr. 1&2

The *International Journal on Advances in Telecommunications* is published by IARIA.

ISSN: 1942-2601

journals site: <http://www.ariajournals.org>

contact: petre@aria.org

Responsibility for the contents rests upon the authors and not upon IARIA, nor on IARIA volunteers, staff, or contractors.

IARIA is the owner of the publication and of editorial aspects. IARIA reserves the right to update the content for quality improvements.

Abstracting is permitted with credit to the source. Libraries are permitted to photocopy or print, providing the reference is mentioned and that the resulting material is made available at no cost.

Reference should mention:

International Journal on Advances in Telecommunications, issn 1942-2601
vol. 9, no. 1 & 2, year 2016, <http://www.ariajournals.org/telecommunications/>

The copyright for each included paper belongs to the authors. Republishing of same material, by authors or persons or organizations, is not allowed. Reprint rights can be granted by IARIA or by the authors, and must include proper reference.

Reference to an article in the journal is as follows:

<Author list>, "<Article title>"
International Journal on Advances in Telecommunications, issn 1942-2601
vol. 9, no. 1 & 2, year 2016, <start page>:<end page>, <http://www.ariajournals.org/telecommunications/>

IARIA journals are made available for free, proving the appropriate references are made when their content is used.

Sponsored by IARIA

www.aria.org

Copyright © 2016 IARIA

Editors-in-Chief

Tulin Atmaca, Institut Mines-Telecom/ Telecom SudParis, France
Marko Jäntti, University of Eastern Finland, Finland

Editorial Advisory Board

Ioannis D. Moscholios, University of Peloponnese, Greece
Ilija Basicovic, University of Novi Sad, Serbia
Kevin Daimi, University of Detroit Mercy, USA
György Kálmán, Gjøvik University College, Norway
Michael Massoth, University of Applied Sciences - Darmstadt, Germany
Mariusz Glabowski, Poznan University of Technology, Poland
Dragana Krstic, Faculty of Electronic Engineering, University of Nis, Serbia
Wolfgang Leister, Norsk Regnesentral, Norway
Bernd E. Wolfinger, University of Hamburg, Germany
Przemyslaw Pochec, University of New Brunswick, Canada
Timothy Pham, Jet Propulsion Laboratory, California Institute of Technology, USA
Kamal Harb, KFUPM, Saudi Arabia
Eugen Borcoci, University "Politehnica" of Bucharest (UPB), Romania
Richard Li, Huawei Technologies, USA

Editorial Board

Fatma Abdelkefi, High School of Communications of Tunis - SUPCOM, Tunisia
Seyed Reza Abdollahi, Brunel University - London, UK
Habtamu Abie, Norwegian Computing Center/Norsk Regnesentral-Blindern, Norway
Rui L. Aguiar, Universidade de Aveiro, Portugal
Javier M. Aguiar Pérez, Universidad de Valladolid, Spain
Mahdi Aiash, Middlesex University, UK
Akbar Sheikh Akbari, Staffordshire University, UK
Ahmed Akl, Arab Academy for Science and Technology (AAST), Egypt
Hakiri Akram, LAAS-CNRS, Toulouse University, France
Anwer Al-Dulaimi, Brunel University, UK
Muhammad Ali Imran, University of Surrey, UK
Muayad Al-Janabi, University of Technology, Baghdad, Iraq
Jose M. Alcaraz Calero, Hewlett-Packard Research Laboratories, UK / University of Murcia, Spain
Erick Amador, Intel Mobile Communications, France
Ermeson Andrade, Universidade Federal de Pernambuco (UFPE), Brazil
Cristian Anghel, University Politehnica of Bucharest, Romania
Regina B. Araujo, Federal University of Sao Carlos - SP, Brazil
Pasquale Ardimento, University of Bari, Italy
Ezendu Ariwa, London Metropolitan University, UK
Miguel Arjona Ramirez, São Paulo University, Brasil
Radu Arsinte, Technical University of Cluj-Napoca, Romania
Tulin Atmaca, Institut Mines-Telecom/ Telecom SudParis, France

Marco Aurelio Spohn, Federal University of Fronteira Sul (UFFS), Brazil
Philip L. Balcaen, University of British Columbia Okanagan - Kelowna, Canada
Marco Baldi, Università Politecnica delle Marche, Italy
Ilija Basicovic, University of Novi Sad, Serbia
Carlos Becker Westphall, Federal University of Santa Catarina, Brazil
Mark Bentum, University of Twente, The Netherlands
David Bernstein, Huawei Technologies, Ltd., USA
Eugen Borcoci, University "Politehnica" of Bucharest (UPB), Romania
Fernando Boronat Seguí, Universidad Politecnica de Valencia, Spain
Christos Bouras, University of Patras, Greece
Martin Brandl, Danube University Krems, Austria
Julien Broisin, IRIT, France
Dumitru Burdescu, University of Craiova, Romania
Andi Buzo, University "Politehnica" of Bucharest (UPB), Romania
Shkelzen Cakaj, Telecom of Kosovo / Prishtina University, Kosovo
Enzo Alberto Candreva, DEIS-University of Bologna, Italy
Rodrigo Capobianco Guido, São Paulo State University, Brazil
Hakima Chaouchi, Telecom SudParis, France
Silviu Ciochina, Universitatea Politehnica din Bucuresti, Romania
José Coimbra, Universidade do Algarve, Portugal
Hugo Coll Ferri, Polytechnic University of Valencia, Spain
Noel Crespi, Institut TELECOM SudParis-Evry, France
Leonardo Dagui de Oliveira, Escola Politécnica da Universidade de São Paulo, Brazil
Kevin Daimi, University of Detroit Mercy, USA
Gerard Damm, Alcatel-Lucent, USA
Francescantonio Della Rosa, Tampere University of Technology, Finland
Chérif Diallo, Consultant Sécurité des Systèmes d'Information, France
Klaus Drechsler, Fraunhofer Institute for Computer Graphics Research IGD, Germany
Jawad Drissi, Cameron University, USA
António Manuel Duarte Nogueira, University of Aveiro / Institute of Telecommunications, Portugal
Alban Duverdiere, CNES (French Space Agency) Paris, France
Nicholas Evans, EURECOM, France
Fabrizio Falchi, ISTI - CNR, Italy
Mário F. S. Ferreira, University of Aveiro, Portugal
Bruno Filipe Marques, Polytechnic Institute of Viseu, Portugal
Robert Forster, Edgemount Solutions, USA
John-Austen Francisco, Rutgers, the State University of New Jersey, USA
Kaori Fujinami, Tokyo University of Agriculture and Technology, Japan
Shauneen Furlong, University of Ottawa, Canada / Liverpool John Moores University, UK
Ana-Belén García-Hernando, Universidad Politécnica de Madrid, Spain
Bezalel Gavish, Southern Methodist University, USA
Christos K. Georgiadis, University of Macedonia, Greece
Mariusz Glabowski, Poznan University of Technology, Poland
Katie Goeman, Hogeschool-Universiteit Brussel, Belgium
Hock Guan Goh, Universiti Tunku Abdul Rahman, Malaysia
Pedro Gonçalves, ESTGA - Universidade de Aveiro, Portugal
Valerie Gouet-Brunet, Conservatoire National des Arts et Métiers (CNAM), Paris
Christos Grecos, University of West of Scotland, UK
Stefanos Gritzalis, University of the Aegean, Greece
William I. Grosky, University of Michigan-Dearborn, USA
Vic Grout, Glyndwr University, UK
Xiang Gui, Massey University, New Zealand
Huaqun Guo, Institute for Infocomm Research, A*STAR, Singapore

Song Guo, University of Aizu, Japan
Kamal Harb, KFUPM, Saudi Arabia
Ching-Hsien (Robert) Hsu, Chung Hua University, Taiwan
Javier Ibanez-Guzman, Renault S.A., France
Lamiaa Fattouh Ibrahim, King Abdul Aziz University, Saudi Arabia
Theodoros Iliou, University of the Aegean, Greece
Mohsen Jahanshahi, Islamic Azad University, Iran
Antonio Jara, University of Murcia, Spain
Carlos Juiz, Universitat de les Illes Balears, Spain
Adrian Kacso, Universität Siegen, Germany
György Kálmán, Gjøvik University College, Norway
Eleni Kaplani, Technological Educational Institute of Patras, Greece
Behrouz Khoshnevis, University of Toronto, Canada
Ki Hong Kim, ETRI: Electronics and Telecommunications Research Institute, Korea
Atsushi Koike, Seikei University, Japan
Ousmane Kone, UPPA - University of Bordeaux, France
Dragana Krstic, University of Nis, Serbia
Archana Kumar, Delhi Institute of Technology & Management, Haryana, India
Romain Laborde, University Paul Sabatier (Toulouse III), France
Massimiliano Laddomada, Texas A&M University-Texarkana, USA
Wen-Hsing Lai, National Kaohsiung First University of Science and Technology, Taiwan
Zhihua Lai, Ranplan Wireless Network Design Ltd., UK
Jong-Hyouk Lee, INRIA, France
Wolfgang Leister, Norsk Regnesentral, Norway
Elizabeth I. Leonard, Naval Research Laboratory - Washington DC, USA
Richard Li, Huawei Technologies, USA
Jia-Chin Lin, National Central University, Taiwan
Chi (Harold) Liu, IBM Research - China, China
Diogo Lobato Acatauassu Nunes, Federal University of Pará, Brazil
Andreas Loeffler, Friedrich-Alexander-University of Erlangen-Nuremberg, Germany
Michael D. Logothetis, University of Patras, Greece
Renata Lopes Rosa, University of São Paulo, Brazil
Hongli Luo, Indiana University Purdue University Fort Wayne, USA
Christian Maciocco, Intel Corporation, USA
Dario Maggiorini, University of Milano, Italy
Maryam Tayefeh Mahmoudi, Research Institute for ICT, Iran
Krešimir Malarić, University of Zagreb, Croatia
Zoubir Mammeri, IRIT - Paul Sabatier University - Toulouse, France
Herwig Mannaert, University of Antwerp, Belgium
Michael Massoth, University of Applied Sciences - Darmstadt, Germany
Adrian Matei, Orange Romania S.A, part of France Telecom Group, Romania
Natarajan Meghanathan, Jackson State University, USA
Emmanouel T. Michailidis, University of Piraeus, Greece
Ioannis D. Moscholios, University of Peloponnese, Greece
Djafar Mynbaev, City University of New York, USA
Pubudu N. Pathirana, Deakin University, Australia
Christopher Nguyen, Intel Corp., USA
Lim Nguyen, University of Nebraska-Lincoln, USA
Brian Niehöfer, TU Dortmund University, Germany
Serban Georgica Obreja, University Politehnica Bucharest, Romania
Peter Orosz, University of Debrecen, Hungary
Patrik Österberg, Mid Sweden University, Sweden
Harald Øverby, ITEM/NTNU, Norway

Tudor Palade, Technical University of Cluj-Napoca, Romania
Constantin Paleologu, University Politehnica of Bucharest, Romania
Stelios Papaharalabos, National Observatory of Athens, Greece
Gerard Parr, University of Ulster Coleraine, UK
Ling Pei, Finnish Geodetic Institute, Finland
Jun Peng, University of Texas - Pan American, USA
Cathryn Peoples, University of Ulster, UK
Dionysia Petraki, National Technical University of Athens, Greece
Dennis Pfisterer, University of Luebeck, Germany
Timothy Pham, Jet Propulsion Laboratory, California Institute of Technology, USA
Roger Pierre Fabris Hoefel, Federal University of Rio Grande do Sul (UFRGS), Brazil
Przemyslaw Pochec, University of New Brunswick, Canada
Anastasios Politis, Technological & Educational Institute of Serres, Greece
Adrian Popescu, Blekinge Institute of Technology, Sweden
Neeli R. Prasad, Aalborg University, Denmark
Dušan Radović, TES Electronic Solutions, Stuttgart, Germany
Victor Ramos, UAM Iztapalapa, Mexico
Gianluca Reali, Università degli Studi di Perugia, Italy
Eric Renault, Telecom SudParis, France
Leon Reznik, Rochester Institute of Technology, USA
Joel Rodrigues, Instituto de Telecomunicações / University of Beira Interior, Portugal
David Sánchez Rodríguez, University of Las Palmas de Gran Canaria (ULPGC), Spain
Panagiotis Sarigiannidis, University of Western Macedonia, Greece
Michael Sauer, Corning Incorporated, USA
Marialisa Scatà, University of Catania, Italy
Zary Segall, Chair Professor, Royal Institute of Technology, Sweden
Sergei Semenov, Broadcom, Finland
Sandra Sendra Compte, Polytechnic University of Valencia, Spain
Dimitrios Serpanos, University of Patras and ISI/RC Athena, Greece
Adão Silva, University of Aveiro / Institute of Telecommunications, Portugal
Pushpendra Bahadur Singh, MindTree Ltd, India
Mariusz Skrocki, Orange Labs Poland / Telekomunikacja Polska S.A., Poland
Leonel Sousa, INESC-ID/IST, TU-Lisbon, Portugal
Liana Stanescu, University of Craiova, Romania
Cosmin Stoica Spahiu, University of Craiova, Romania
Young-Joo Suh, POSTECH (Pohang University of Science and Technology), Korea
Hailong Sun, Beihang University, China
Jani Suomalainen, VTT Technical Research Centre of Finland, Finland
Fatma Tansu, Eastern Mediterranean University, Cyprus
Ioan Toma, STI Innsbruck/University Innsbruck, Austria
Božo Tomas, HT Mostar, Bosnia and Herzegovina
Piotr Tyczka, ITTI Sp. z o.o., Poland
John Vardakas, University of Patras, Greece
Andreas Veglis, Aristotle University of Thessaloniki, Greece
Luís Veiga, Instituto Superior Técnico / INESC-ID Lisboa, Portugal
Calin Vlădeanu, "Politehnica" University of Bucharest, Romania
Benno Volk, ETH Zurich, Switzerland
Krzysztof Walczak, Poznan University of Economics, Poland
Krzysztof Walkowiak, Wrocław University of Technology, Poland
Yang Wang, Georgia State University, USA
Yean-Fu Wen, National Taipei University, Taiwan, R.O.C.
Bernd E. Wolfinger, University of Hamburg, Germany
Riaan Wolhuter, Universiteit Stellenbosch University, South Africa

Yulei Wu, Chinese Academy of Sciences, China
Mudasser F. Wyne, National University, USA
Gaoxi Xiao, Nanyang Technological University, Singapore
Bashir Yahya, University of Versailles, France
Abdulrahman Yarali, Murray State University, USA
Mehmet Erkan Yüksel, Istanbul University, Turkey
Pooneh Bagheri Zadeh, Staffordshire University, UK
Giannis Zaoudis, University of Patras, Greece
Liaoyuan Zeng, University of Electronic Science and Technology of China, China
Rong Zhao , Detecon International GmbH, Germany
Zhiwen Zhu, Communications Research Centre, Canada
Martin Zimmermann, University of Applied Sciences Offenburg, Germany
Piotr Zwierzykowski, Poznan University of Technology, Poland

CONTENTS

pages: 1 - 12

Control Plane Design and Implementation for a Media Streaming System Working in Over the Top Style

Eugen Borcoci, University POLITEHNICA of Bucharest, Romania

Serban Georgica Obreja, University POLITEHNICA of Bucharest, Romania

Cristian Cernat, University POLITEHNICA of Bucharest, Romania

Radu Iorga, University POLITEHNICA of Bucharest, Romania

Jordi Mongay Batalla, National Institute of Telecommunications, Poland

Daniel Negru, University of Bordeaux, France

pages: 13 - 24

A Step Forward on Adaptive Iterative Clipping Approach for PAPR Reduction in OFDM System

Lamarana Mamadou Diallo, CentraleSupélec, France

Jacques Palicot, CentraleSupélec, France

Faouzi Bader, CentraleSupélec, France

pages: 25 - 34

Radio Resource Allocation for Indoor Secondary Access in TV White Space

Mohamed Hamid, University of Agder, Norway

Niclas Björsell, University of Gävle, Sweden

Control Plane Design and Implementation for a Media Streaming System working in Over the Top style

Eugen Borcoci, Serban Georgica Obreja, Cristian Cernat,
Radu Iorga
University POLITEHNICA of Bucharest
Bucharest, Romania
emails: eugen.borcoci@elcom.pub.ro,
serban@radio.pub.ro, cristian.cernat@elcom.pub.ro,
radu.iorga@elcom.pub.ro

Jordi Mongay Batalla
National Institute of Telecommunications
Warsaw, Poland
email:jordim@interfree.it
Daniel Negru
LaBRI Lab, University of Bordeaux
Bordeaux, France
email:daniel.negru@labri.fr

Abstract — Content/media streaming services are frequently used in the current Internet and this trend is estimated to continue in the next years. Complex architectures, like Content Delivery Networks, have been developed and are currently exploited on a large scale, or novel architectures like Content Oriented Networks are proposed. In parallel, cheaper and light architecture, working in over-the-top (OTT) style above the current IP networks multi-domain infrastructures have been recently considered, as an attractive solution for media distribution. A content streaming OTT-like system is considered here, working on top of a multi-domain IP network. The system integrates functionalities such as content server initial selection based on multi-criteria algorithm and then performs dynamic media adaptation and/or server switching - during the media session. This paper continues and extends a preliminary work; it presents more deeply the main design concepts, then develops the implementation solutions and presents the functional conformance testing for the Control Plane of the above system. The functional testing is described, performed on a real-life multi-domain testbed as a part of the overall validation campaign.

Keywords — Content delivery, Dynamic Adaptive Streaming over HTTP, Monitoring, Server and Path selection.

I. INTRODUCTION

In the current Internet, content/media streaming services are frequently used and this trend is estimated to continue in the next years. Several approaches are encountered in practice: light and cheap over-the-top (OTT) solutions like that described in [1] or complex ones, the latter being usually based on powerful and costly management system. Complex architectures like Content Delivery Networks [2], have been developed and are currently exploited on a large scale, or novel architectures like Content Oriented Networks (CON) [3][4], are proposed.

Some cheaper and light over-the-top (OTT) solutions are recently proposed and developed for media/content delivery, where the services are delivered over the current Internet by an entity called Service Provider (SP). The SP is not directly responsible for the quality of the flow transmission to the

end-user. The users have access to the services via the “public Internet”. An OTT SP could exist as a separate entity from traditional Internet Service Provider (ISP), or might be embedded in ISP. Also, combined solutions exist, with OTT Service Providers using the Content Delivery Network (CDN) Providers’ infrastructure to improve the quality of delivery.

A light (OTT-like) novel architecture for content streaming systems over the current Internet is proposed by the European DISEDAN Chist-Era project [1][5], (*service and user-based Distributed SElection of content streaming source and Dual Adaptation*N, 2014-2015).

This paper is an extension work of a previous one [1] presented at AICT 2015 Conference, dedicated to develop the design of the Control Pane system of the DISEDAN project. The present work goes further, towards full implementation and system functional testing. The additional material is contained mainly in the Sections V and VI.

The business actors involved are: *Service Provider (SP)* - an entity/actor which delivers the content services to the users and possibly owns and manages the transportation network; *End Users (EU)* consumes the content; a *Content Provider (CP)* could exist, owning some *Content Servers (CS)*.

The DISEDAN project proposed an evolutionary solution to enhance the content delivery via Internet. It has been focused on research in the area of multi-criteria content source (server) selection and handover, considering user and server contexts. Two main concepts have been studied and implemented: *two-step server initial selection mechanism* and *dual adaptation in-session mechanism*.

The “Two-step server initial selection mechanism”, is run before the media session start. It allows for cooperation between Service Provider (an entity offering the content distribution service, owning or not a network infrastructure) and End User, making use of innovative server selection algorithms that consider context- and content-awareness. A solution is proposed for the (multi-criteria-hard) problem of best content source (server) selection, considering user context, servers’ availability and requested content.

The “Dual adaptation mechanism” is activated during the media session. It is based on combining in a single

solution the advantages of Media (flow rate) adaptation methods and/or content server handover.

At client side the proposed streaming system is able to function as a standalone client application, without any modifications applied to the Service Provider (SP). However in DISEDAN the SP is supposed to be able to provide to the client a list of available and appropriate servers. This additional information is helpful for the initial client decision, thus optimizing the initial server selection. Consequently, a set of optional Provider side modifications have been identified and implemented (w.r.t. useful information and metrics provided by SP to the client) (see [14]) that can further optimize server selection. The design of the system took the backwards-compatibility into consideration, ensuring that each of the client-side and Service Provider - side modifications works well with the other side, while the dialogue partner (SP/client) is using existing content distribution solutions.

In [14] clear rules for deciding which adaptation action to perform have been defined, based on the evaluated current delivery conditions. Possibilities of inferring the optimum adaptation decision by estimating network state from various client measurements have been studied.

The research results have been verified by performing tests of the prototype implementation of the solution. These are partially reported in this paper. The system implementation can be released as open source client library which will allow other institutions to reproduce the results and continue future investigations on these issues. Simulation models have been elaborated [5], during the project and the associated experiments have been run to complement the implementation - based tests, in order to assess the scalability of the proposed solutions in the context of large networks and users communities.

Note that DISEDAN system management does not deal with contractual CP-SP relationships; therefore one may assume that CSs are also owned by the SP. Our solution consisting in: (1) *two-step server selection mechanism* (at SP and at EU) using and (2) *dual adaptation mechanism* consisting of *dynamic media adaptation* and/or *content source switching* (by *streaming server switching*) could be rapidly deployed in the market since it does not require complex architecture like Content Delivery Networks [2], or Content Oriented Networking [3][4].

The *Dynamic Adaptive Streaming over Hypertext Transfer Protocol- HTTP (DASH)* technology has been selected for in-session media adaptation. The DASH was recently adopted as multimedia streaming standard, to deliver high quality multimedia content over the Internet, by using conventional HTTP Web servers [6] - [10]. It uses the HTTP protocol, minimizes server processing power and is video codec agnostic. Its basic concept is to enable automatic switching of quality levels according to network conditions, user requirements, and expectations.

A DASH client continuously selects the highest possible video representation quality that ensures smooth play-out, in the current downloading conditions. This selection is performed on-the-fly, during video play-out, from a pre-

defined discrete set of available video rates and with a pre-defined granularity (according to video segmentation).

The DASH offers important advantages (over traditional push-based streaming), like: significant market adoption of HTTP and TCP/IP protocols to support the majority of the today Internet services; HTTP-based delivery avoids NAT and firewall- related issues; the HTTP-based (non-adaptive) deployment of progressive download existing today, can be conveniently be upgraded to support DASH; the ability to use standard/existing HTTP servers and caches instead of specialized streaming servers allows reuse of the existing infrastructure.

The work of this paper is dedicated to continue the design, following the decisions presented in [1] (for details of the major design decisions one can see [14]), for a light Control Plane (CPI) of the OTT streaming system and develop the implementation. Functional testing framework and results are outlined in a dedicated section.

Note that implementation of the DASH adaptation details are not in the scope of this paper.

A special attention has been paid for the Monitoring subsystem (MON), whose components are developed at SP, CS and optionally at EU Terminal (EUT). The MON is an essential functional component, contributing to the evaluation of the QoS and QoE and charged to trigger appropriate actions if it is the case. The information delivered by MON is used to support both the initial server selection and then in-session actions.

Note that our main purpose in this work has not been to essentially innovate in monitoring tools (a lot of implementations are available), but to integrate different components, aiming to develop a complete monitoring subsystem appropriate for DISEDAN light architecture.

The paper structure is described here. Section II is a short overview of related work. Section III outlines the overall architecture and problem description. Section IV is focused on defining CPI design decisions and implementation-related implications. Section V presents the main implementation characteristics. Section VI defines a testbed to support the system and presents samples of functional tests results. Section VII contains conclusions and future work outline.

II. RELATED WORK

The real-time adaptation in content streaming is a powerful and dynamic technique, adopted to solve the fluctuations in QoE/QoS. One can classify adaptation as acting on Media (flow) and/or on Content Server. The *Media adaptation* is a significant technique and constitutes a main research and innovation area in media streaming applications [7][8][15]. *CS adaptation* means a new content server selection (during the media session) and switching (handover), depending on the consumer device capabilities, consumer location, content servers state and/or network state [11][12].

A so-called “dual adaptation” is a process that integrates the above adaptation methods. The DISEDAN novel architecture [5] combines the initial server selection (result of cooperation between SP and EU) with session-time dual adaptation, in a single solution.

The initial server selection is based on optimization algorithms like *Multi-Criteria Decision Algorithms (MCDA)* [11][12], or *Evolutionary Multi-objective Optimization algorithm (EMO)* [13], modified to be applied to DISEDAN context. In these works several scenarios are proposed, analyzed and evaluated. In particular, the availability of different static and/or dynamic input parameters for optimization algorithms is considered. The result of this variability is that several CPI designs are possible, different in terms of performance and complexity. The dynamic capabilities for the initial CS selection and then for adaptation decisions depends essentially on the power of the DISEDAN monitoring system. Different design variants, offering actually a family, have been in detail analyzed in [14].

The challenge in DISEDAN is to combine the DASH-related functionalities with additional monitoring in order to finally realize the dual adaptation.

The standard ISO/IEC 23009-1, "Information technology -- Dynamic adaptive streaming over HTTP (DASH)" [8], defines the DASH-Metrics client reference model, composed of *DASH access client (DAC)*, followed by the *DASH-enabled application (DAE)* and *Media Output (MO)* module. The DAC issues HTTP requests (for DASH data structures), and receives HTTP request responses. Consequently three observation points (interfaces – I/F) can be identified (see Figure 1) :

- *O1 at network-DAC I/F*: a set of TCP connections, each defined by its destination IP address, initiation, connect and close times; a sequence of transmitted HTTP requests, each defined by its transmission time, contents, and the TCP connection on which it is sent; and for each HTTP response, the reception time and contents of the response header and the reception time of each byte of the response body.

- *O2 at DAC-DAE I/F*: consists of encoded media samples. Each encoded media sample is defined as: media type; decoding time; presentation time; the @id of the Representation from which the sample is taken; the delivery time.

- *O3 at DAE-MO I/F*: consists of decoded media samples. Each decoded media sample is defined as: the media type; the presentation timestamp of the sample (media time); the actual presentation time of the sample (real time); the @id of the Representation from which the sample is taken (the highest dependency level if the sample was constructed from multiple Representations).

A summary of the metrics semantic defined in ISO/IEC 23009-1 [8], is: *Transmission Control Protocol (TCP) connections, HTTP request/response transactions, Representation switch events, Buffer level, Play list*. A similar list of QoE metrics standardized by 3GPP defined in 3GPP in 26.247, applicable for DASH, [10][15], contains: *HTTP request/ response transactions; Representation switch events; Average throughput; Initial play-out delay; Buffer level; Play list; MD information*.

For completeness of the text, the full architecture of the DISEDAN system is presented in the following sections; however the focus here is on server selection functionality.

III. DISEDAN SYSTEM ARCHITECTURE

This section shortly presents the system architecture, starting with the general framework and assumptions and then outlining the general functional architecture.

A. General framework and assumptions

The definition and details of the system architecture are already given in [5][11][12][14]. In this section, a summary only will be presented, to facilitate the understanding of the Control Plane design decisions.

The main business entities/ actors are those already mentioned in Section I: Service Provider (SP), End User (EU) and Content Server (CS). In practice there can exist another distinct entity, Content Provider (CP), which is the normal owner the Content Servers. However, considering the OTT- style and simplified design of our system, the SP and Content Provider (CP) entities are not seen as distinct. Also, a full CS management is out of scope of this system. The connectivity between CSs and EU Terminals (EUT) is assured by traditional *Internet Services Providers (ISP) / Network Providers (NP)* - operators. The ISP/NPs whose networks are crossed by the media flows might or not to have business relationships but these are not visible in the management DISEDAN architecture.

However, the DISEDAN solution can be also emedded in more complex business models, e.g., involving Cloud Providers, CDN providers, etc. The relationships between SP and such entities could exist, but their realization is out of scope of this study. While Service Level Agreements (SLAs) might be agreed between SP and ISPs/NPs, related to connectivity services offered by the latter to SP, such SLAs are not directly visible at DISEDAN system level.

The system can work over the traditional TCP/IP mono and/or multi-domain network environment. The EUTs are not supposed to have explicit knowledge about the managed/non-managed characteristics of the connectivity services. No reservation for connectivity resources, neither connectivity services differentiation at network level are explicitly supposed (they might exist or not). This architectural choice proves the system flexibility: it can work in OTT style, or over a managed connectivity service offered by the network. Therefore, the SP does not commit to offer strong QoS guarantees for the streaming services provided to EUs. Consequently, DISEDAN does not suppose, but does not exclude, establishment of a SLA relationships between EUs and SPs management entities. However, it is assumed that a Media Description Server exists, managed by SP, to which EUT will directly interact.

The media streaming actions are independent on the transport networking technology. The EUT part (client side) works as a standalone client application, without any mandatory modifications applied to the SP; however, SP should provide some basic information to EUT, to help it in making initial server selection (and optionally to help in-session CS switching). The in-session decision about dual adaptation (media flow adaptation and/or CS switching) will be taken mainly locally at EUT, thus assuring complete User

independency and avoiding complex signaling in the Control Plane, between EUT and SP during the session.

An assumption is made in our system: several CSs might exist, known by SP (geographical location, server availability level, access conditions for users). Among them, the SP and/or EUs can operate server selection (initial phase) and/or switching (in-session action).

The DISEKAN system research study has been limited to innovative parts. The proposed architecture does not treat how to solve failures inside the networks, except attempts to perform media flow DASH adaptation or CS switching when the service quality observed at EU is too low. The proposed system does not explicitly treat or innovate in the domain of content protection, Digital Rights Management (DRM), etc., but might use currently available solutions. Billing, financial aspects and other business related management of the DISEKAN high level services are out of the project scope.

The work [14], elaborated also in DISEKAN framework, has defined all requirements coming for EU, SP and out of them derived the general and specific System requirements, together with some assumptions and constrains imposed to such a system. The resulting high level architecture has been determined by such requirements. This work is based on the assumption of fulfillment of those requirements.

B. General Architecture

Figure 1 shows a simplified high level view of the general architecture.

The Control Plane at SP includes the following functional modules:

- *MPD File generator* – dynamically generates Media Presentation Description (MPD) XML file,

containing media segments information (video resolution, bit rates, etc.), ranked list of recommended CSs and, optionally - current CSs state information and network state (if applicable).

- *Selection algorithm* –runs Step 1 of server selection process. It exploits *MCDA* [11][12], modified to be applied to DISEKAN context, or *EMO* [13], etc., to rank the set of recommended CSs and media representations, while aiming to optimize servers’ load as well as to maximize system utilization.
- *Monitoring module* – collects monitoring information from CSs and performs the processing required to estimate the current state of each CS. Note that if some EU information should go to SP, then this information is transited (and aggregated) from EUT via CS towards SP.

The End User Terminal (EUT) entity includes the modules:

- *Data Plane: DASH (access and application)* – parses the MD file received from SP and handles the download of media segments from CS; *Media Player* – playbacks the downloaded media segments.
- *Control Plane: Content Source Selection and Adaptation engine* –implements the dual adaptation mechanism; *Selection algorithm* – performs the Step 2 of server selection process. It can also exploit MCDA, EMO, or other algorithms to select the best CS from the set of candidates recommended by SP; *Monitoring module* – monitors the changes in the local network and server conditions.

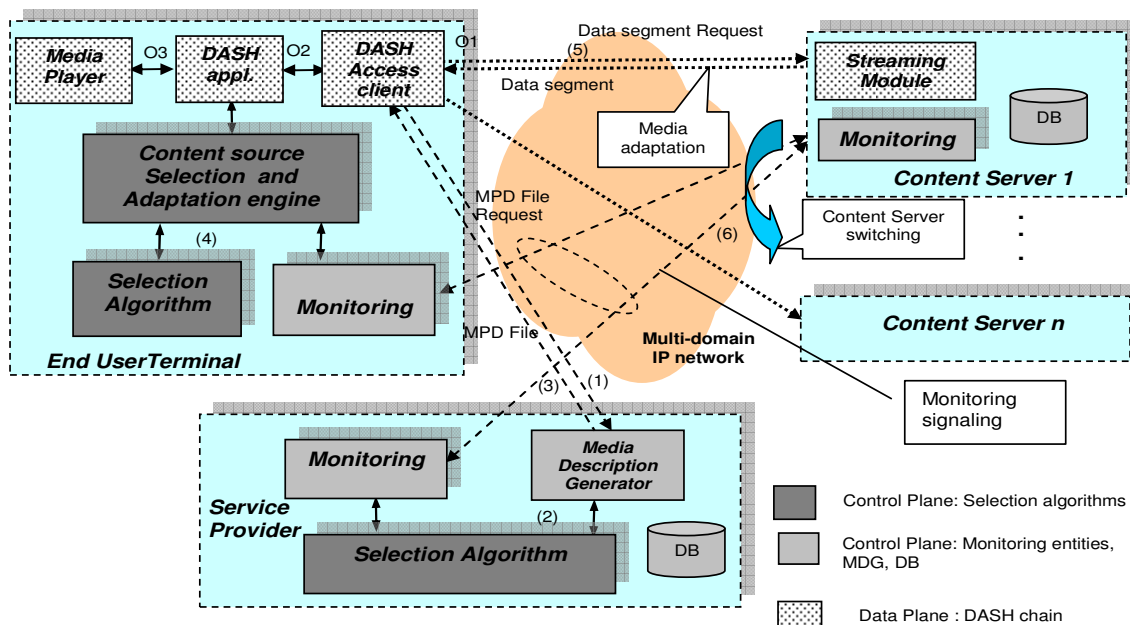


Figure 1. DISEKAN general architecture; DASH - Dynamic Adaptive Streaming over HTTP; MD – Media Description; DB – Data Base ; O1, O2, O3 – DASH Observation Points [ISO/IEC 23009-1]

The Content Server (CS) entity includes the modules:

- *Data Plane: Streaming module* – sends media segments requested by End Users.
- *Control Plane: Monitoring module* – monitors some CS performance metrics (CPU utilization, network interfaces utilization, etc.). In a complex implementation of the CS, the monitoring can evolve from a simple metering probe to an advanced monitoring module, capable to supervise not only the active sessions but also some connectivity characteristics from this CS to different groups of users.

Figure 1 also shows the following operational steps (simplified description):

- (1) EUT issues to SP a media file request.
- (2) SP analyzes the status of the CSs and runs the MCDA/EMO selection algorithm (optionally the SP could make first, a current probing of the CSs). For each user request the SP could consider also the user profile, the policies of the SP for this user's class and other information at the SP side (e.g., state of the servers and possibly network-related information).
- (3) SP returns to EUT a ordered list of candidates CS (this is the SP proposal embedded in a MD- xml file).
- (4) The EUT performs the final CS selection, by running its own selection algorithm. This can have as input local informations available at EUT.
- (5) The EUT starts asking video segments from the selected CS.

During media session the EUT makes quality and context measurements. Continuous media flow adaptation is applied using DASH technology if necessary, or (6) CS switching is decided.

From the EU point of view, the steps 1-2-3 composed the so-called Phase1 and steps 4-5-6 the Phase 2.

During the receipt of consecutive chunks, the user's application can automatically change the rate of the content stream (internal DASH actions - which are out of scope in this paper) and/or also can switch to another CS. When EUT receives requested segments, it performs measurements to monitor parameters of download process. Note that the system is flexible in terms of monitoring procedures to follow. For instance, if EUT detects deterioration of the downloading rate, it can use SP information about alternate CSs and/or it can start probing other CSs. When the probing process is finished, EUT starts the dual adaptation process to decide: either DASH-based media adaptation, or server adaptation (i.e. server switching). If the first is selected, then EU downloads (via DASH) next segments with reduced rate, otherwise it switches to another CS (CS probing by te EUT might be involved in such an action).

IV. MONITORING SUBSYSTEM

The architecture of the DISEDAN CPI is flexible. Several variants/versions of designs can be considered, i.e., a basic one or more complex, essentially depending on the roles of the business entities and their capabilities, interactions and also on SP and EU policies. The selection algorithms MCDA/EMO might work with different sets of static and/or dynamic input parameters. An important component of the CPI is the Monitoring subsystem (*MON@DISEDAN*).

A. Monitoring Architecture

Three MON modules have been identified in Figure 1: *MON@SP*, *MON@CS*, *MON@EUT*. However, not all these entities must participate to all operational phases. The variety of solutions will determine the system overall performance, but with additional cost for the more complex solutions. The monitored data are used to accomplish the following macro objectives:

- guide the initial server selection at SP and (optionally) at EU,
- guide the media adaptation and/or CS switching.

From the EUT point of view, two phases are distinguished: *Phase1* in which the EUT is not connected to any CS, but it just tries to do this, by contacting the SP; *Phase2* in which the EUT is currently served by a CS (media session time). The monitored data at EU level are different in Phase 1 w.r.t. Phase 2.

Note also that during media session, the DASH subsystem performs its own evaluation of the QoE and, based on this, decides upon requested rate of the next video segment. The implementation of this type of monitoring is out of MON scope. However, the data collected from such on-line monitoring can be combined with other values delivered by *MON@EU* and delivered to other entities in the hierarchy (CS, SP). Actually, we adopted the approach described in [15] where it is recalled that in the 3GPP DASH specification TS 26.247 [7-8], QoE measurement and reporting capability is defined as an optional feature for client devices. If the EUT supports the QoE reporting feature, the DASH standard also mandates the reporting of all of the requested metrics at any given time; that is, the client should be capable of measuring and reporting all of the QoE metrics specified in the standard.

The standard TS 26.247 also specifies two options for the activation or triggering of QoE reporting:

- a. via the Quality Metrics element in the MPD;
- b. via the OMA Device Management (DM) QoE Management Object.

In both cases a and b, the trigger message from the CS would include reporting configuration information such as the set of QoE metrics to be reported, the URIs for the server(s) to which the QoE reports should be sent, the format of the QoE reports, information on QoE reporting frequency and measurement interval, percentage of sessions for which QoE metrics will be reported, and access point

names to be used for establishing the packet data protocol (PDP) context to be used for sending the QoE reports.

The selection algorithms MCDA/EMO might work with different sets of static and/or dynamic input parameters.

To achieve scalability of the monitoring system an important design decision is to avoid direct signaling between EUT and SP, except the initial request issued by EUT towards SP, in order to get the MPD xml file. Apart this phase, any monitored information obtained in EUT premises will be sent to the current CS serving that EUT.

Three control bi-directional channels are defined (see Figure 1) :

EUT-SP to generate the EU request to SP and to get the MPD file from SP. This is performed in Phase 1 of the DISEDAN functional cycle, i.e., at CS selection time.

EUT-CS triggered by the serving CS, to report, the monitored data about current EU status and media session data. This signaling is performed during Phase 2 time life for this EUT (i.e., media session).

CS-SP- to report: CS status data (capacity occupied, number of connections currently served, etc.); status data received from EUT (such data can be related to some individual users or aggregated at the CS level. The communication on this channel is triggered by the SP.

B. Typical Scenarios

Figure 2 presents a simplified Message Sequence Chart (MSC) illustrating the activities, communication in Data Plane (DASH) and the associated signaling executed in the Control Plane. One can see the Phase 1 and Phase 2 sets of actions, performed by EUT1.

Several types of monitoring activities are performed, described below.

Proactive monitoring: executed in some continuous mode (at SP level and possibly at EUT level- see the “loop” notations in Figure 2); such information is input for the CS selection algorithm (Phase 1), when some new content requests arrive from a given EU to SP. At SP, this means supervision of different servers, maybe networks, and user communities, depending on its policies. SP/CS cooperation on this purpose is envisaged. Such data can be also used to construct a history and updated status of the environment envisaged by the SP. The CSs could be involved in proactive monitoring, provided they are capable to probe the connectivity characteristics towards different groups of users (indicated by the SP).

At EU side, proactive monitoring might be performed, depending on capabilities of the EUT and its SW. In some more complex scenarios the EU can construct history, dedicated to its usual content connections (if they are estimated to be repeated in the future). The terminal context can be evaluated by such measurements, including its access network status.

In-session monitoring: it is performed on a single media flow and measured results are collected in real time, to assess the level of QoS/QoE observed at EU side.

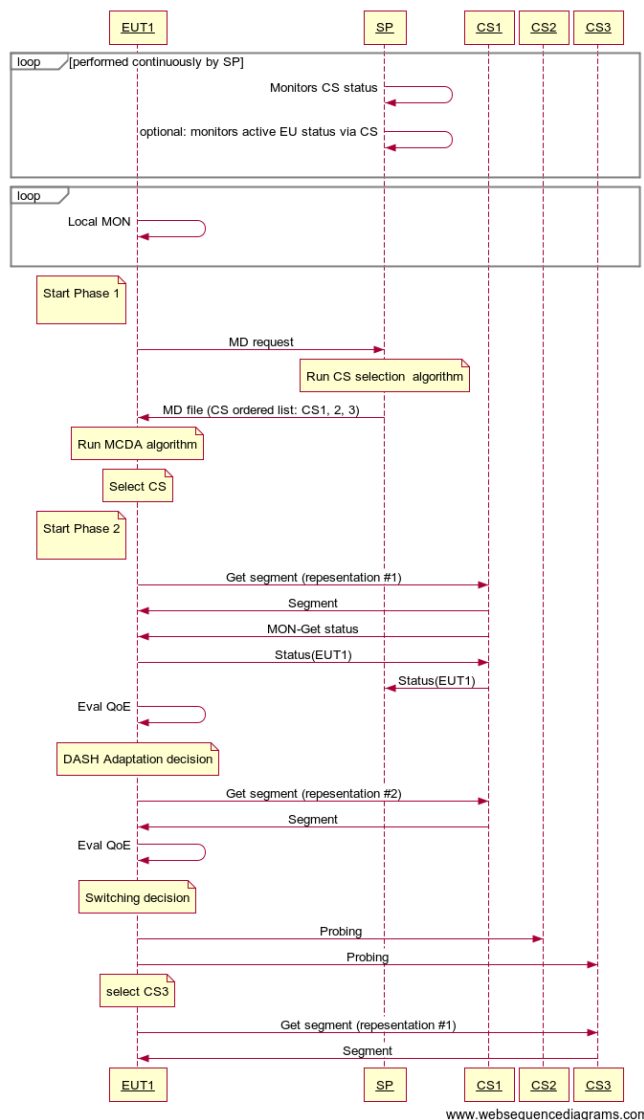


Figure 2. Typical activity and signaling diagram

Note that two kind of information are produced:

- collected by the DASH mechanisms, to serve internally as real time inputs to adaptation decision engine at EU;
- collected by the MON@EUT, which can be consolidated with those produced by the DASH, thus offering a more complete view not only about the reception of the media flow but also on general status and environment of the EUT.

In more complex DISEDAN variants, the SP and/or CS can be involved in such monitoring, at least in being aware of results (note that no SLA concerning mutual obligations of SP/EUs, related to QoE are established in DISEDAN system): for all active users or subsets; for all monitored data or summaries; full or summary monitored values.

Opportunity related monitoring: measurements essentially performed by the EUT to test the opportunity of

switching the CS that delivers the content to EU. An example of such category is the probing action of some CS candidates if a CS switching action is prepared.

C. Metrics and MON versions

Apart from DASH defined metrics (in-session observed), the MON subsystem may collect information on:

MON@EUT: CS accessibility (probing); EUT local dynamic context; historical and prediction data on servers and paths utilization.

MON@SP: CS status (collected from CS); active Users status; current load on some paths (here the network monitoring of the NP should cooperate); other dynamic characteristics of some paths (e.g., loss, jitter); historical and prediction data on servers and paths utilization.

MON@CS: CS status (load); CS environment data (network paths, connectivity paths dynamic characteristics - evaluated at overlay level – where paths are considered from CS to different groups of users; EUTs data, active user groups data.

Therefore the overall MON system design is flexible, since it can combine different features of the above components.

V. IMPLEMENTATION

SP and CS will have an internal database that will contain monitored and/or post-processed data. Also these two entities will be capable to send and receive JSON messages embedded in simple HTTP calls. EU might not

have any internal database; it will just have the basic capability to send only simple HTTP calls to either SP or CS.

For Database it has decided to use *PostgreSQL*, technology [18]. The *PostgreSQL* is a powerful, open source object-relational database system. It runs on all major operating systems, including Linux, UNIX, and Windows.

SP and CS must be able to receive and send simple HTTP messages to each other. For this reason it is needed a web server and a programming language to implement these features. Web server of choice is Node.js [19].

The *Node.js* [19] is an open source, cross-platform runtime environment for server-side and networking applications. The *Node.js* applications are written in JavaScript, and can be run within the *Node.js* runtime on OS X, Microsoft Windows, Linux and FreeBSD.

VI. FUNCTIONAL TESTING

This section presents the functional testing approach and samples of results. To illustrate the real implementation proof of working, some details of the messages collected during test scenarios are inserted. For readers interested in testing philosophy only, such details could be skipped.

A. Experimental testbed

An experimental laboratory testbed has been built as hardware support for DISEDAN functionalities validation, as presented in Figure 3.

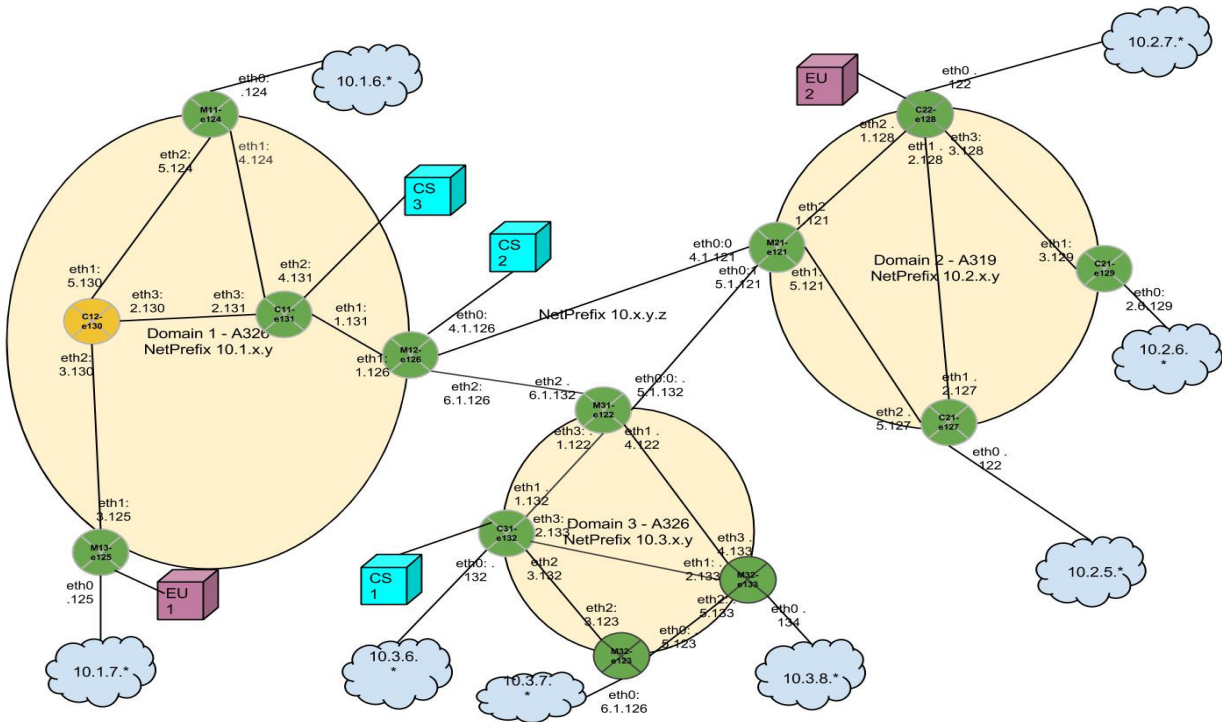


Figure 3. Experimental test-bed structure (multi-domain network)

The system comprises three independent IP network domains, equivalent to some core networks, each of them equipped with several core and edge/border routers (Linux based). No QoS technologies at network layer are active in these networks. Several DISEDAN entities are connected to this network: SP, EU, CS through some access networks. Note that the presence of the access networks in the overall system is not essential, given the OTT-style of work of the system.

B. Functional conformance tests(for initial phase server selection)

The first set of tests has been defined and executed in order to check the correctness of Control Plane. Samples are given below for illustrative purposes. More complete results can be found in [20].

DISEDAN_CT_1 (Unit-level functional testing)

Objective: to assess the functional correctness of each (individual) module. The information messages sent and received by modules are captured and allow to understand the correctness of the steps that each module takes in order to perform its DISEDAN task.

Conditions: the individual component runs and information messages are collected. The software entities irrelevant for the given module under test might not be active (e.g., EUT can run even if monitoring on CS is down; SP should just returns a list of servers).

DISEDAN__CT_2 (System level functional testing)

Objective: to assess the functional correctness of modules cooperation (i.e. the entire DISEDAN signaling chain). Example (simplified) : EUT send a request; SP asks monitoring; Monitoring responds; SP runs MCDA aselection algorithm; SP answers to EUT; The EUT runs its MCDA again; EUT gets content.

Conditions: all the components run in a complete DISEDAN assembly. Info messages are also collected. The difference from the first TC is that now all the software entities should be up and running.

- **CT_1 Results:**

The following sample sequence of messages shows the results of the test CT1:

- **EUT Functional testing results**

```
requestServerList: url =
http://141.85.43.130:5000/getserver/1001
parseServerList:
```

```
CS address: 141.85.43.132
CS address: 141.85.43.131
CS address: 141.85.43.129
```

```
getServersInfo:
```

```
Open Thread for CS 141.85.43.132
Open Thread for CS 141.85.43.131
Open Thread for CS 141.85.43.129
```

```
getNetworkInfo: Get network information for CS 141.85.43.132
```

```
getNetworkInfo: Get network information for CS 141.85.43.131
```

```
getNetworkInfo: Get network information for CS 141.85.43.129
```

```
RTT for 141.85.43.131 is 2.14
```

```
RTT for 141.85.43.132 is 2.17
```

```
Hop Count for 141.85.43.132 is 16
```

```
Hop Count for 141.85.43.131 is 16
```

```
141.85.43.129 is down
```

```
getBestServer:
```

```
MCDA Matrix created:
```

```
1 0.5 0
0.988182 0.988485 0
1.11111 1.11111 0
```

```
MCDA:
```

```
best server is 141.85.43.132
```

```
accessContent:
```

```
vlc
```

```
http://141.85.43.132/bunny\_1s/BigBuckBunny\_1s\_isoffmain\_DS\_23009\_1\_v\_2\_1c2\_2011\_08\_30.mpd
```

The above sequence proves the correct Control Plane signaling at EUT level.

CT_2 Test:

The basic signalling and message exchange have been tested. The sequence of steps is illustrated in Figure 4:

1. The EUT requests a streaming service from SP. The request contains the ID of the media service requested.

2. The SP gets from its local database the identity of the servers hosting the requested content. Using its monitoring module, the SP interrogates the monitoring agents located on the CSs about the CS state. The main monitoring parameters collected by SP are: CS processor load, CS free memory (normalized at the total memory), number of streaming processes on CS, total bandwidth on the network interface.

3. After receiving the monitoring parameters, the SP selects, using the MCDA, the best servers from the list of servers hosting the requested resource.

4. An ordered list of selected servers is returned to EUT. The best server from SP's point of view is placed on the first position in the list.

- 5-6. The EUT performs a second selection step. The *Round Trip Time (RTT)* and the distance in terms of *hop count* is measured from EUT to the CSs in the list recommended by SP. The communication on step 5 is performed only with the servers selected by SP. Based on this metric, the best server is finally selected by EUT.

Final step: the EUT requests the service from the selected CS, which start to stream packets towards the EUT.

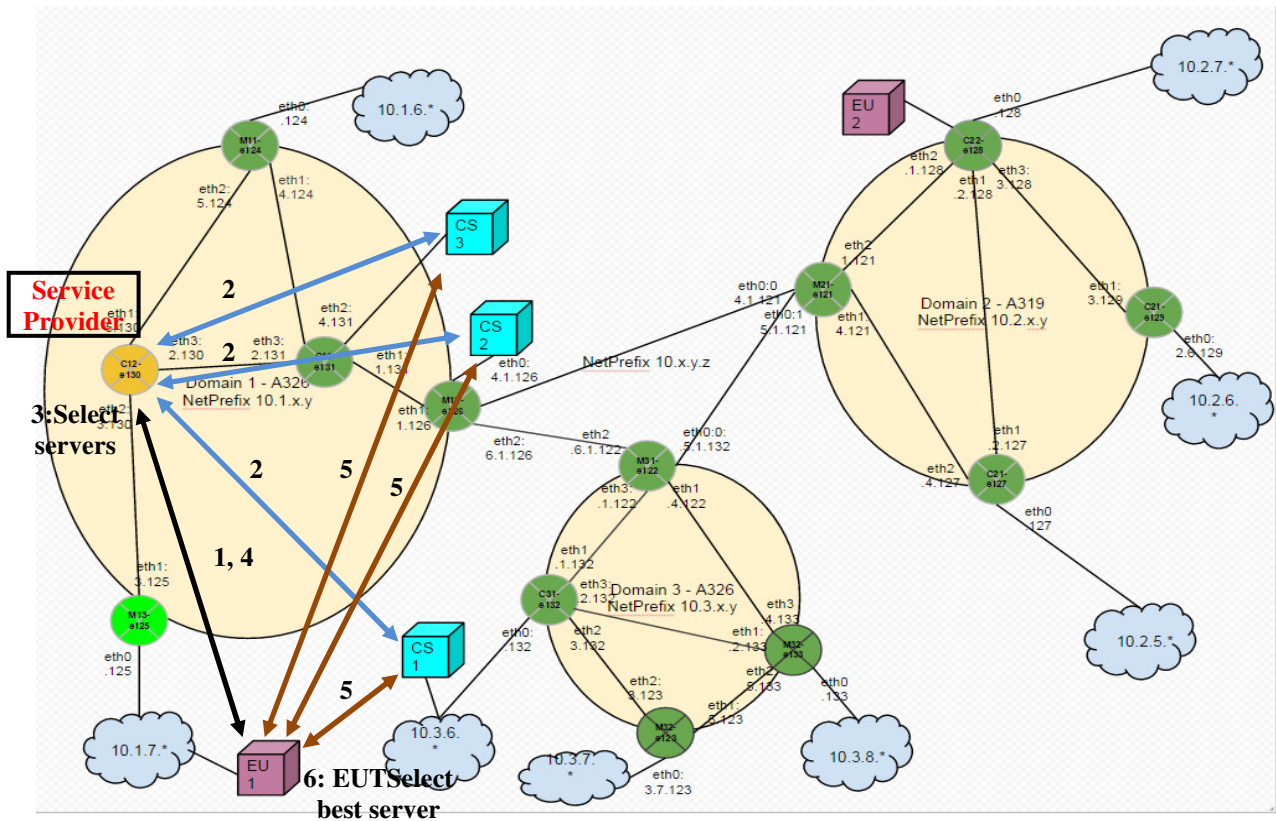


Figure 4. The steps of the functional validation for server selection in DISEDAN testbed

All the functional steps described above have been validated by capturing and analyzing the messages exchanged between EUT, CS, SP.

The following sample sequence of messages shows the results of the test CT_2:

- **EUT functional testing results**
Messages captured on the EUT terminal:

```
al@e125:~/disedan/project_disedan/DisedanEndUser/bin$ ./DisedanEndUser
```

```
STEP1: requestServerList: url = http://141.85.43.130:5000/getserver/100
STEP 4: parseServerList:
```

```
CS address: 10.3.6.132
CS address: 10.1.1.126
```

```
STEP5: getServersInfo:
Open Thread for CS 10.3.6.132
Open Thread for CS 10.1.1.126
```

```
getNetworkInfo: Get network information for CS 10.1.1.126
getNetworkInfo: Get network information for CS 10.3.6.132
```

```
RTT for 10.1.1.126 is 0.593
RTT for 10.3.6.132 is 0.999
Hop Count for 10.1.1.126 is 5
Hop Count for 10.3.6.132 is 7
```

```
STEP 6:
getBestServer:
Matrix created:
```

```
1.5 1
1.00001 1.00411
0.333333 0.555556
```

```
MCDA:
best server is 10.1.1.126
```

```
STEP 7: accessContent:
vlc
http://10.1.1.126/bunny_1s/BigBuckBunny_1s_isoffmain_DIS_230
09_1_v_2_1c2_2011_08_30.mpd
VLC media player 2.2.0-rc2 Weatherwax (revision 2.2.0-rc1-118-
g22fda39)
[0000000000992118] core libvlc: Running vlc with the default
interface. Use 'cvlc' to use vlc without interface.
```

- **Messages captured at the SP:**

```
(flask)root@e130:~/serban/microblog# python
sp_server_monitoring.py
```

INFO:werkzeug: * Running on http://0.0.0.0:5000/ (Press CTRL+C to quit)

STEP 1:
Got request from 10.1.7.125 for resource with ID = 100
[Service Provider]: List of servers hosting resource id = 100 :
 ['10.1.4.131', '10.3.6.132', '10.1.1.126']

STEP 2:
[Service Provider]: Network distance list between user and CSes:
 [4, 6, 3]

INFO:requests.packages.urllib3.connectionpool:Starting new HTTP connection (1): 10.1.4.131
DEBUG:requests.packages.urllib3.connectionpool:"GET /loadavg HTTP/1.1" 200 None
INFO:requests.packages.urllib3.connectionpool:Starting new HTTP connection (1): 10.3.6.132
DEBUG:requests.packages.urllib3.connectionpool:"GET /loadavg HTTP/1.1" 200 None
INFO:requests.packages.urllib3.connectionpool:Starting new HTTP connection (1): 10.1.1.126
DEBUG:requests.packages.urllib3.connectionpool:"GET /loadavg HTTP/1.1" 200 None
[Service Provider]: CS servers' LOAD list:
 [0.0146484375, 0.0146484375, 0.0146484375]

INFO:requests.packages.urllib3.connectionpool:Starting new HTTP connection (1): 10.1.4.131
DEBUG:requests.packages.urllib3.connectionpool:"GET /system_status?proc=apache HTTP/1.1" 200 None

INFO:requests.packages.urllib3.connectionpool:Starting new HTTP connection (1): 10.3.6.132
DEBUG:requests.packages.urllib3.connectionpool:"GET /system_status?proc=apache HTTP/1.1" 200 None
INFO:requests.packages.urllib3.connectionpool:Starting new HTTP connection (1): 10.1.1.126
DEBUG:requests.packages.urllib3.connectionpool:"GET /system_status?proc=apache HTTP/1.1" 200 None
[Service Provider]: CS servers' number of Apache processes list:
 [4, 4, 4]

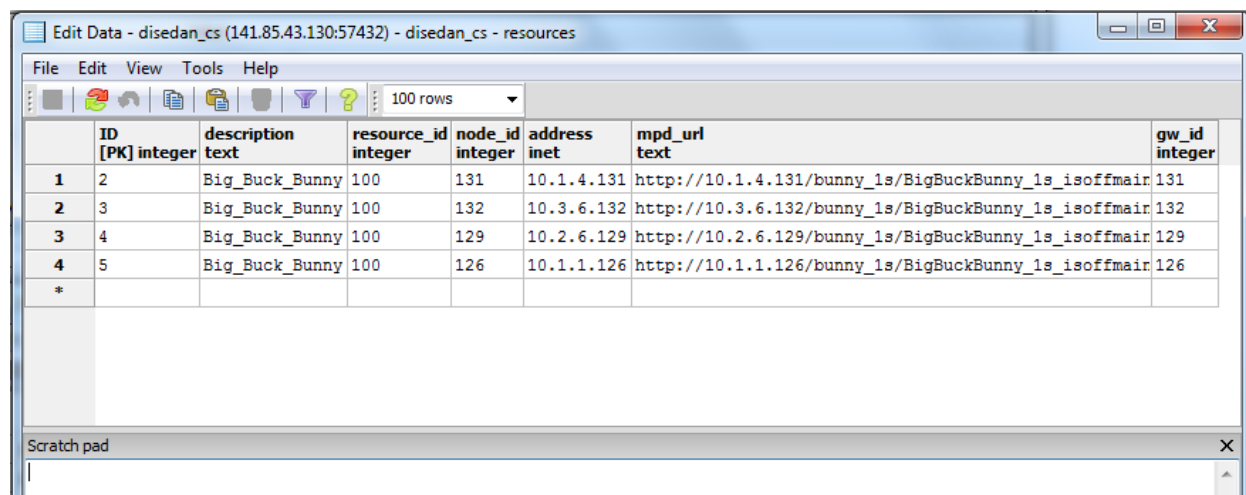
.....
 Monitoring system – samples of results

The monitoring system has been implemented with two components: a static component and a dynamic one. The static component deals with some static information about the network, content servers and terminals. These data are related to the configuration of the system and are stored in the system's database. They are statically inserted in the database in the initialization phase. The second component is the dynamic one and consists in a monitoring module running at SP and monitoring agents running on each content server. Whenever a new request is received by SO, the monitoring module connects to the monitoring agents requesting monitoring data about the content servers.

Some examples of monitoring data are given below. Figure 5 shows the list of network distances between the access networks known by SP. Figure 6 shows the list of media object resources available at different CSs as they are known at SP level.

ID [PK]	integer	node_id_source integer	distance integer	node_id_destination integer	is_egress_source boolean	is_ingress_source boolean	address_source inet	address_destination inet
1	8	125	80	131	TRUE	FALSE	10.1.7.0/24	10.1.4.0/24
2	9	125	25	132	TRUE	FALSE	10.1.7.0/24	10.3.6.0/24
3	10	125	28	129	TRUE	FALSE	10.1.7.0/24	10.2.6.0/24
4	11	128	18	131	TRUE	FALSE	10.2.1.0/24	10.1.4.0/24
5	12	128	25	132	TRUE	FALSE	10.2.1.0/24	10.3.6.0/24
6	13	128	29	129	TRUE	FALSE	10.2.1.0/24	10.2.6.0/24
7	14	125	70	126	TRUE	FALSE	10.1.7.0/24	10.1.1.0/24
8	15	128	17	126	TRUE	FALSE	10.2.1.0/24	10.1.1.0/24
*								

Figure 5. The list of network distances between the access networks known by the SP



	ID [PK] integer	description text	resource_id integer	node_id integer	address inet	mpd_url text	gw_id integer
1	2	Big_Buck_Bunny	100	131	10.1.4.131	http://10.1.4.131/bunny_1s/BigBuckBunny_1s_isoffmair	131
2	3	Big_Buck_Bunny	100	132	10.3.6.132	http://10.3.6.132/bunny_1s/BigBuckBunny_1s_isoffmair	132
3	4	Big_Buck_Bunny	100	129	10.2.6.129	http://10.2.6.129/bunny_1s/BigBuckBunny_1s_isoffmair	129
4	5	Big_Buck_Bunny	100	126	10.1.1.126	http://10.1.1.126/bunny_1s/BigBuckBunny_1s_isoffmair	126
*							

Figure 6. List of resources hosted by the content servers

VII. CONCLUSIONS AND FUTURE WORK

This paper continued the work presented in [1]. It detailed the design concepts, and exposed the guidelines for system implementation of a *media delivery system having a light-architecture and working on top of the current Internet connectivity*. Functional testing for the Control Plane has been described.

Given the complexity of the overall DISEDAN system, the focus of this work was on a part of the system, i.e., the initial content server selection functionality, as preliminary phase of the media session (including media adaptation and/or CS switching) for media consumption. The architectural specification has been refined, then the Control Plane design is described. Implementation characteristics are shortly presented. Finally, some samples of conformance tests results (performed on a real-life testbed) are given, proving the correctness of the Control Plane behavior. It has been checked that the SP correctly performs the initial server selection by running an MCDA algorithm, and delivers to the client an ordered list of servers. Monitoring-related functions have been also tested for conformance.

Experimental results on performances will be reported in other papers.

Future work will be done to evaluate the possibility to extend the DISEDAN architecture for media distribution in the context of wireless and 4G/5G environment, where distributed caching in the access networks is envisaged. Such an environment will be favorable for DISEDAN-like solution in media streaming applications.

ACKNOWLEDGMENT

This work has been partially supported by the Research Project DISEDAN, No.3-CHIST-ERA C3N, 2014- 2015.

REFERENCES

- [1] E. Borcoci, C. Cernat, and R. Iorga, "Control Plane Design for a Content Streaming System with Dual Adaptation," AICT 2015 Conference, https://www.thinkmind.org/index.php?view=article&articleid=aict_2015_6_40_10154
- [2] P. A. Khan and B. Rajkumar, "A Taxonomy and Survey of Content Delivery Networks," Department of Computer Science and Software Engineering, University of Melbourne, Australia: s.n., 2008. www.cloudbus.org/reports/CDN-Taxonomy.pdf.
- [3] J. Choi, J. Han, E. Cho, T. Kwon, and Y. Choi, "A Survey on Content-Oriented Networking for Efficient Content Delivery," IEEE Communications Magazine, March 2011, pp. 121-127.
- [4] "Information-Centric Networking-3," Dagstuhl Seminar, July 13-16 2014, <http://www.dagstuhl.de/en/program/calendar/semhp/?seminar=14291>, [retrieved: February, 2015].
- [5] <http://wp2.tele.pw.edu.pl/disedan/> [retrieved: May, 2015]
- [6] T. Dreier, "Netflix sees cost savings in MPEG DASH adoption," 15 December 2011. [Online]. Available: <http://www.streamingmedia.com/Articles/ReadArticle.aspx?ArticleID=79409>, [retrieved: October, 2014].
- [7] I. Sodagar, "The MPEG-DASH Standard for Multimedia Streaming Over the Internet," MultiMedia, IEEE, vol. 18, no. 4, 2011, pp. 62 - 67.
- [8] ISO/IEC 23009-1, "Information technology -- Dynamic adaptive streaming over HTTP (DASH) -- Part 1: Media presentation description and segment formats," ISO/IEC, Geneva, second edition, 2014.
- [9] 3GPP TS 26.247 v10.1.0, "Transparent End-to-End Packet Switched Streaming Service (PSS); Progressive Download and Dynamic Adaptive Streaming Over HTTP (3GP-DASH)," Release 10, June 2011.
- [10] ETSI TS 126 247 V11.7.0 (2014-07) (UMTS); LTE; Transparent end-to-end Packet-switched Streaming Service (PSS); Progressive Download and Dynamic Adaptive Streaming over HTTP (3GP-DASH), (3GPP TS 26.247 version 11.7.0 Release 11, 2014).
- [11] A. Beben, J. M. Batalla, W. Chai and J. Sliwinski, "Multi-criteria decision algorithms for efficient content delivery in

- content networks,” *Annals of Telecommunications - annales des telecommunications*, Springer, vol. 68, Issue 3, 2013, pp. 153-165.
- [12] E. Borcoci, M. Vochin, M. Constantinescu, J. M. Batalla, and D. Negru, “On Server and Path Selection Algorithms and Policies in a light Content-Aware Networking Architecture,” *ICSNC 2014 Conference*, <http://www.elcom.pub.ro/disedan/docs/ICSNC%202014%20Conf.pdf>.
- [13] J. M. Batalla, C.X. Mavromoustakis, G. Mastorakis, D. Négru and E. Borcoci, “Evolutionary Multiobjective Optimization algorithm for two-phase content source selection process in Content Aware Networks,” submitted to *Springer 4OR - A Quarterly Journal of Operations Research*.
- [14] E. Borcoci, ed., et al., D2.1 “System requirements and comparative analysis of existing solutions for media content server selection and media adaptation,” July 2014, <http://wp2.tele.pw.edu.pl/disedan>.
- [15] O. Oyman and S. Singh, “Quality of Experience for HTTP Adaptive Streaming Services,” *IEEE Communications Magazine*, April 2012, pp. 20-27.
- [16] C. Alberti, D. Renzi, C. Timmerer, C. Mueller, S. Lederer, S. Battista and M. Mattavelli, “Automated QoE Evaluation of DASH,” 2013 Fifth International Workshop on Quality of Multimedia Experience (QoMEX), <http://infoscience.epfl.ch/record/188813/files/p20-Alberti.pdf>, [retrieved: February, 2015].
- [17] C. Müller, S. Lederer and C. Timmerer, “An Evaluation of Dynamic Adaptive Streaming over HTTP in Vehicular Environments,” www-itec.uni-klu.ac.at/dash/?p=517.
- [18] <http://www.postgresql.org>, [retrieved: March, 2015].
- [19] <http://nodejs.org>, [retrieved: March, 2015].
- [20] S.Obreja, E.Borcoci ed., et al., D3.3 “Results of conformance tests,” January 2016, <http://wp2.tele.pw.edu.pl/disedan>

A Step Forward on Adaptive Iterative Clipping Approach for PAPR Reduction in OFDM System

Lamarana Mamadou Diallo

Jacques Palicot

Fauzi Bader

CentraleSupélec/IETR/SCEE
Avenue de la Boulaie-CS 47601
35576 Cesson-Sévigné Cedex, Rennes,
France
Mamadou-Lamarana.Diallo@supelec.fr

CentraleSupélec/IETR/SCEE
Avenue de la Boulaie-CS 47601
35576 Cesson-Sévigné Cedex, Rennes,
France
jacques.palicot@centralesupelec.fr

CentraleSupélec/IETR/SCEE
Avenue de la Boulaie-CS 47601
35576 Cesson-Sévigné Cedex, Rennes,
France
faouzi.bader@supelec.fr

Abstract—The Orthogonal Frequency Division Multiplexing (OFDM) is the most commonly used multicarrier modulation in telecommunication systems because of its efficient use of frequency resources and its robustness to multipath fading channels. However, as any multicarrier signal, the Peak-to-Average-Power Ratio (PAPR) is one of the major drawbacks of OFDM signals. Many research papers have dealt with the PAPR mitigation methods, such as clipping methods, tone reservation based approaches, and partial transmit signals. However, in this paper we focus on the clipping method. This method is one of the most efficient adding signal techniques for PAPR reduction in terms of complexity. Nevertheless, clipping presents many drawbacks such as a bit error rate degradation, an out-of-band emission, and a mean power degradation. In this paper, a clipping method featuring a threshold that adapts to the desired upper bounded output PAPR is presented. Once the desired output PAPR has been predefined, the proposed AC approach consists of clipping each OFDM symbol with an adaptive threshold so that the PAPR value of the clipped symbol is equal to this desired output PAPR. This paper proposes three different ways to compute the adaptive threshold of each OFDM symbol we want to clip according to the desired output PAPR. The theoretical analysis and the simulation results validate the interest and potential of this new clipping method.

Keywords—Orthogonal Frequency Division Multiplexing; High Power Amplifier; Peak-to-Average Power Ratio; Complementary Cumulative Distribution Function; Clipping; Adaptive Clipping

I. INTRODUCTION

The work presented by the authors in the previous AICT 2016 conference in Bruxelles [1], was focusing on the reduction of the complexity of the Adaptive Clipping (AC) method, previously presented in [2]. The present paper extends the work in [1] by introducing a new way to compute the adapted algorithm to reach the targeted PAPR. The proposed work, allows to reach the exact solution of the problem, whereas the computed threshold in [1] and in [2] just allows to get an approximation. Furthermore, we illustrate, in this paper, the achieved performances by extensive results, which prove the interest of our proposal.

The Peak-to-Average Power Ratio (PAPR) is one of the main issues of the Orthogonal Frequency Division Multiplex (OFDM) signal [3]. Many works such as the coding based techniques [4], [5], the probabilistic based approaches [6], [7] and the "adding signal for high peak cancellation" based

techniques [8], [9], [10] have been documented in the literature for the purpose of PAPR mitigation. The clipping method [11], [12] is an efficient technique for PAPR mitigation where the peak-cancellation signal is computed thanks to the clipping of the signal amplitudes that exceed a predefined threshold A . This paper focuses on classical clipping method (CC), detailed in [11]. The main objective of the presented is to propose a new clipping technique that offers better outcomes than that of the CC methods in terms of signal degradation, and similar outcomes in terms of PAPR reduction. In others words, the proposed clipping method achieves:

- 1) A better bit error rate (BER), a lesser out-of-band (OOB) emission and mean power degradation.
- 2) Same performances in terms of PAPR reduction.

Note that, in practice, in CC method, a normalized threshold is used: $\rho = 10 \log_{10} \left(\frac{A^2}{P_x} \right)$, where P_x represents the mean power of the discrete signal x , whose PAPR has to be reduced. It can be noted that the normalized threshold defines the PAPR, below which the signal is not clipped. Due to the large amplitude variations of the OFDM signals in the time domain, the PAPR value of each OFDM symbol highly depends on its content. Therefore, after achieving the PAPR mitigation thanks to the CC method [11] by featuring a predefined normalized threshold, the obtained PAPR value also depends on its content. Therefore, the upper bounded PAPR of the clipped signal, at each value of its Complementary Cumulative Distribution Function (CCDF), increases when the CCDF decreases. This is illustrated by the left curve depicted in Fig. 1. Note that this is also the case for the original OFDM CCDF curve. That means that there is no deterministic upper bounded PAPR for CC method. This is exactly what we target in this work. This deterministic value corresponds to the vertical solid blue line depicted in Fig. 1.

In practice, the suitable upper bounded PAPR value of the signal for the Input Back Off (IBO) definition at the High Power Amplifier (HPA) is chosen where $CCDF(\Phi)$ is close to zero (usually 10^{-4}). In this paper, which is an extension of the work presented in [1], this value is called the desired upper bounded PAPR and denoted as $PAPR_0$. Thus, in [1], [2] the authors have shown that in CC method many OFDM symbols are either severely clipped or unnecessarily clipped with respect to this desired upper bounded $PAPR_0$. To illustrate

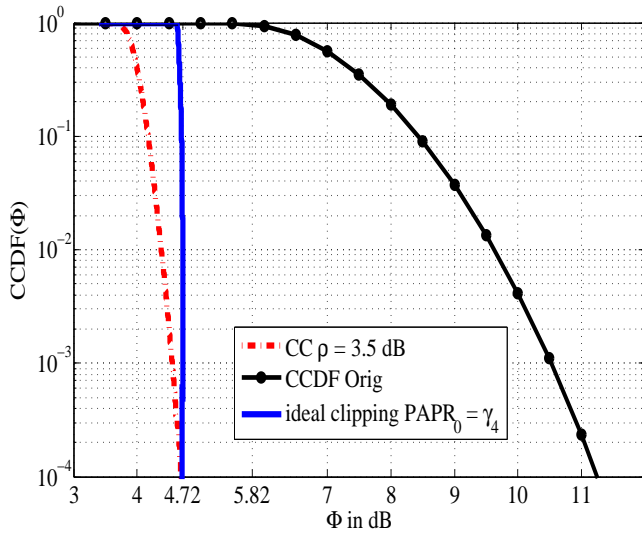


Figure 1. Scenario of the CCDF curves of a CC and Ideal Clipping.

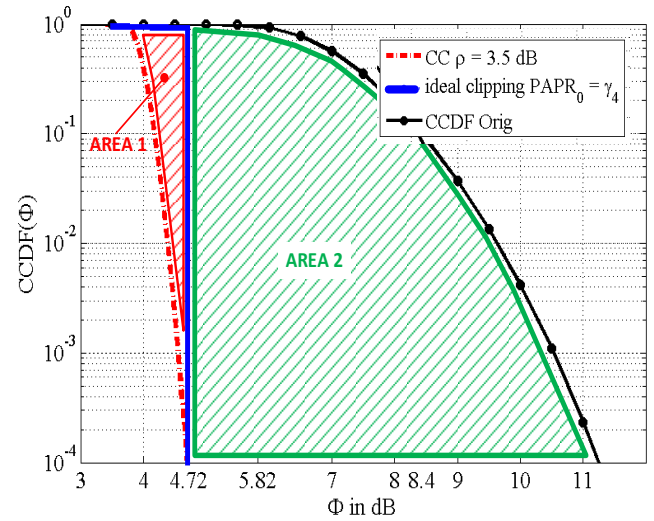


Figure 3. Scenario of the CCDF curves of a CC and Ideal Clipping. AREA1: symbols unnecessarily clipped, AREA2: symbols clipped more severely than necessary.

this assertion, let us depict in Fig. 2 the result of zooming the zone around 10^{-1} for the CCDF in Fig. 1. Note that our main objective is to have a PAPR clipping output whose value is close to 4.72 dB (the vertical blue line). Therefore, all the symbols that have a PAPR value between 4.1 dB and 4.72 dB are clipped unnecessarily (see Δ_1 in Fig. 2). Besides this, all the symbols whose PAPR values are between 4.72 dB and 8.4 dB are too severely clipped by the CC technique in comparison with the ideal clipping (indicated by Δ_2 in Fig. 2). If we extend these considerations to all CCDF values, we then obtain the two areas indicated in Fig. 3 as:

- Area1: symbols are unnecessarily clipped
- Area2: Symbols are clipped more severely than necessary

In order to avoid these drawbacks, the authors have pro-

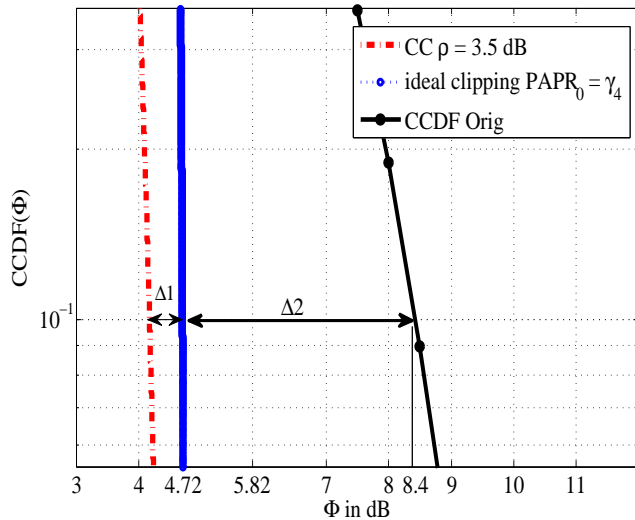


Figure 2. Zoom at $CCDF=10^{-1}$ to illustrate symbols too much clipped by CC.

posed an AC algorithm in [1], [2], where the threshold is adapted to the content of each OFDM symbol, according to the desired upper bounded PAPR value $PAPR_0$. Other AC methods exist in the literature [13], [14]. In [14], the authors proposed to adapt the normalized threshold ρ depending on the mapping constellation of the OFDM signal for a better compromise between the PAPR reduction and the BER degradation. In [13], the authors proposed an adaptive iterative clipping and filtering scheme [15], in which the computation of the amplitude threshold A , is first computed on the basis of the predefined normalized threshold, and done at each iteration. This latter approach improves the performances of the system in terms of PAPR reduction but further degrades the signal. In contrast, in [2], the proposed AC approach and the CC method [11] achieve similar performance in terms of PAPR reduction. However, a better bit error rate (BER), a lesser out-of-band (OOB) emission, and a lesser mean power degradation are achieved. Nevertheless, the computational complexity of the proposed algorithm is high. In fact, an exhaustive search, by means of a constant step (ϵ) is performed, so as to find the optimal threshold. Therefore, the number of required iterations to find the optimal threshold $\rho^{(x)}$ will depend on both the content of each OFDM symbol and the step ϵ .

In [1], a fast AC method has been proposed to compute the value of $\rho^{(x)}$. Presented approach consists of adapting the step ϵ at each iteration to the content of each OFDM symbol, this is equivalent to clip the signal iteratively by adapting the clipping magnitude at each iteration as a function of $PAPR_0$ and the content of the clipped signal at the previous iteration. Therefore, this approach requires less iterations to find the adaptive threshold [2]. This approach is called the Iterative Adaptive Clipping (IAC). The AC and IAC methods give both an approximation of the adaptive threshold ρ^x via an exhaustive search featuring respectively a constant and a non constant step. This paper is an extension of the analysis presented in [1], where we will first provide a complete analysis of both the AC and IAC methods. Then, we will

extend our analysis to present a new approach that allows us to find the exact adaptive threshold ρ^x . This new approach is named power approximation based method for adaptive clipping (PAC).

The paper is organized as follows: In Section II, the problem's formulation of the AC principle will be briefly presented. In Sections III-A and III-B, we will review the AC and the IAC approaches and we will show that IAC method needs fewer iterations than AC approach so as to reach $\rho^{(x)}$. In Section (III-C) the new proposed approach will be presented. A comparative study pertaining to signal degradation will then be conducted in Section IV. Finally, conclusions will be presented in Section V.

II. PROPOSED APPROACH PRINCIPLE

In this section, after reminding some definitions and notations, the AC method is hereafter described.

A. Notations and definitions

Throughout this paper an OFDM symbol $x(t)$ of duration T_u is given by the following equation

$$x(t) = \sum_{m=0}^{M-1} X_m e^{j2\pi m F t}, \text{ with } 0 \leq t \leq T_u, \quad (1)$$

where M is the total number of carriers, $F = \frac{1}{T_u}$ is the inter-carrier space, mF the m^{th} frequency, and X_m the symbol carried out by the m^{th} carrier at time T_u .

We denote $\mathbf{x} = [x_0, \dots, x_{LM-1}]$ the vector containing the discrete samples of $x(t)$ after the oversampling operation. It has been demonstrated that it can be efficiently computed thanks to use of Inverse Fast Fourier Transform (IDFT)¹. As described in [16], since the PAPR mitigation operation is generally undertaken in the discrete time domain, the oversampling factor L should be greater than 4 in order to get a good approximation of the PAPR of the analogue OFDM symbol $x(t)$. The PAPR value of \mathbf{x} is given by the following expression

$$\text{PAPR}_{[\mathbf{x}]} = \frac{\max_{m=0, \dots, ML-1} \{|x_m|^2\}}{P_{\mathbf{x}}}, \quad (2)$$

where $P_{\mathbf{x}}$ is the mean power of the discrete OFDM symbol \mathbf{x} .

Since \mathbf{x} is a random variable, the Complementary Cumulative Distribution Function (CCDF) defined by (3) is used to characterize the useful upper bounded PAPR for the IBO's characterization. In practice, this upper bounded PAPR value can be chosen at $\text{CCDF}_{(\cdot)}(\Phi) = 10^{-4}$ as

$$\text{CCDF}_{\mathbf{x}}(\Phi) = \mathbb{P}\text{rob} [\text{PAPR}_{[\mathbf{x}]} \geq \Phi] \quad (3)$$

In this paper, this upper bounded PAPR value will be denoted by γ_4 and will be referred to as the achieved PAPR or output PAPR. Note that, in our proposed approach, this value will be denoted by PAPR_0 . More generally, the positive scalar γ_e will represent in this paper the upper bounded PAPR of symbols

obtained at a clip rate of 10^{-e} , i.e., at the CCDF value equal to 10^{-e} with $e \geq 0$

$$\gamma_e = \max_{\Phi} \{ \text{CCDF}_{\mathbf{y}}(\Phi) \geq 10^{-e} \}, \quad (4)$$

where $\text{CCDF}_{\mathbf{y}}(\Phi) = \mathbb{P}\text{rob}[\text{PAPR}_{[\mathbf{y}]} \geq \Phi]$ and $\mathbf{y} = [y_0, \dots, y_{ML-1}]$ is the OFDM symbol after clipping.

B. The proposed AC approach principle

The CC proposed in [11] is one of the most popular clipping technique for PAPR reduction known in the literature. It is sometimes called hard clipping or soft clipping. To avoid any confusion, the term CC will be used thereafter in this paper. In [11], its effects on the performance of OFDM, which include the determination of the power spectral density, the PAPR and the BER, are evaluated. The function-based clipping, used in CC technique, is defined as

$$f(r, A) = \begin{cases} r, & r \leq A \\ A, & r > A \end{cases}, \quad (5)$$

where A is the magnitude clipping threshold. From (5) we can say that, if some samples of \mathbf{x} are greater than the clipping threshold A , then the PAPR value of the output signal \mathbf{y} , obtained after PAPR reduction that uses the CC method, can be expressed as follows

$$\text{PAPR}_{\mathbf{y}} = \frac{A^2}{P_{\mathbf{y}}}. \quad (6)$$

Given, $A = (10^{\frac{\rho}{20}}) \sqrt{P_{\mathbf{x}}}$, the PAPR of \mathbf{y} can be rewritten as follows:

$$\text{PAPR}_{\mathbf{y}} = \left(10^{\frac{\rho}{20}}\right) \left(\frac{P_{\mathbf{x}}}{P_{\mathbf{y}}}\right) \\ \text{then } \text{PAPR}_{\mathbf{y}}(\text{ in dB }) \geq \rho(\text{ in dB }). \quad (7)$$

Therefore, it can be noticed that $\gamma_e \geq \rho$ for any $e \geq 0$. Thus, γ_e increases where e increases. In practice, the desired γ_e for the IBO parametrization at the HPA is generally chosen where the CCDF value is equal to 10^{-4} , i.e., γ_4 . Then, it worth remarking that the CC method can lead to the fact that many OFDM symbols are clipped more severely than necessary or are unnecessarily clipped with respect to γ_4 [2]. Fig. 3 shows the zones representing the set of OFDM symbols that are clipped more severely than necessary (AREA2) or unnecessarily clipped (AREA1), when we use a CC method featuring $\rho = 3.5$ dB so as to reduce their PAPR, with respect to Ideal Clipping (see vertical blue line of Fig. 3), and for the same upper bounded PAPR obtained at a CCDF value equal to 10^{-4} (γ_4). The vertical blue line represents the ideal clipping CCDF where $\text{PAPR}_0 = \gamma_4$, which corresponds to the deterministic desired upper bounded PAPR. It is obvious that the output upper bounded PAPR of such an ideal clipping is constant at any value of the CCDF. The main goal of the proposed AC approach is to come close to the ideal clipping. Therefore, AC will degrade less the signal after clipping than the CC method, and features similar performances than that of the latter in terms of PAPR reduction. Hence, once the desired upper bounded PAPR₀ and an OFDM symbol \mathbf{x} featuring an initial PAPR value greater than PAPR₀ have been obtained, the proposed AC approach consists of two stages:

- 1) Computation of the adaptive threshold $\rho^{(x)}$.

¹In this paper, we use the zero-inserting scheme to calculate \mathbf{x} , i.e., the IDFT operation is applied to the extended vector $\tilde{\mathbf{X}} = [X_0, \dots, X_{\frac{M}{2}-1}, \underbrace{0, \dots, 0}_{(L-1)M \text{ zeros}}, X_{\frac{M}{2}}, \dots, X_{M-1}]$.

Having determined the $PAPR_0$ value, the signal \mathbf{x} needs to be clipped. On that basis, the AC method consists firstly in finding $\rho^{(x)}$ so that the PAPR value of \mathbf{y} , obtained after clipping \mathbf{x} featuring $\rho^{(x)}$, is equal to $PAPR_0$. In other words, the AC method consists of adapting the clipping threshold $\rho^{(x)}$ of each OFDM symbol \mathbf{x} that we want to clip with according to the desired upper bounded PAPR value, i.e., $PAPR_0$. Therefore, this stage consists of solving the following equation

$$PAPR_0 = \gamma_4 = \left(10^{\frac{\rho^{(x)}}{10}}\right) \left(\frac{P_x}{P_y}\right), \quad (8)$$

where P_y is the mean power of the clipped signal \mathbf{y} .

- 2) Clip the OFDM symbol \mathbf{x} as in (5) thanks to its adaptive threshold $\rho^{(x)}$.

From (7), it can be noticed that P_y depends on the unknown parameter ρ_n . Therefore, solving (8) is not a trivial problem. Thus, the main challenge of the AC is the computation of the adaptive threshold for each OFDM symbol. In [1], [2], two approaches based on a exhaustive search are proposed, so as to approximate the adaptive threshold. These approaches will be reviewed more clearly hereafter in Section III-A and Section III-B, respectively.

The following section presents a complete analysis of the AC and IAC method [1] and the description of the new proposed approaches for the computation of the adaptive threshold $\rho^{(x)}$.

III. THE ADAPTIVE THRESHOLD COMPUTATION

After having described the AC method principle in the previous section, we propose, here, a complete analysis of three different methods for computing the adaptive threshold.

A. Comprehensive search carried out by means of a constant step: AC method

As it is noticed in Section II, the computation of the adaptive threshold for each OFDM symbol is not a trivial problem since the mean power P_y of the clipped symbol depends on the unknown $\rho^{(x)}$, see (8). In order to bypass this difficulty, the authors propose in [2] to find an approximation of $\rho^{(x)}$ thanks to a exhaustive search within the interval $[0, PAPR_0]$. In fact, from (7) it can be noticed that, for each value of $PAPR_0$ and \mathbf{x} that we want to clip, their adaptive threshold is less than $PAPR_0$. Besides, if ρ_1 and ρ_2 are two clipping thresholds such that $(\rho_1 - \rho_2)$ is close to zero, the PAPR values of the clipped OFDM symbols using these thresholds are approximately equal. Thus, where $\epsilon > 0$ and $\delta > 0$, the authors propose to check successively $\rho_0 = \gamma_4$, $\rho_1 = \rho_0 - \epsilon$, \dots , $\rho_m = \rho_{m-1} - \epsilon, \dots$, to reach $\rho^{(x)}$, which satisfies

$$(\gamma_4 - PAPR_y) \leq \delta \quad (9)$$

Fig. 4 describes the chart of the adaptive threshold computation. In the rest of the paper, this approach will be named the AC method. From Fig. 4, it can be noted that, for each OFDM symbol \mathbf{x} featuring with a PAPR value greater that $PAPR_0$, the PAPR value $PAPR_{[y]}$ obtained after a clipping process featuring its adaptive threshold ρ^x is less than $PAPR_0 + \delta$. Thus, if δ is sufficiently small, then $PAPR_y \simeq PAPR_0$. Therefore, the CCDF curve of the AC method will approach the CCDF curve

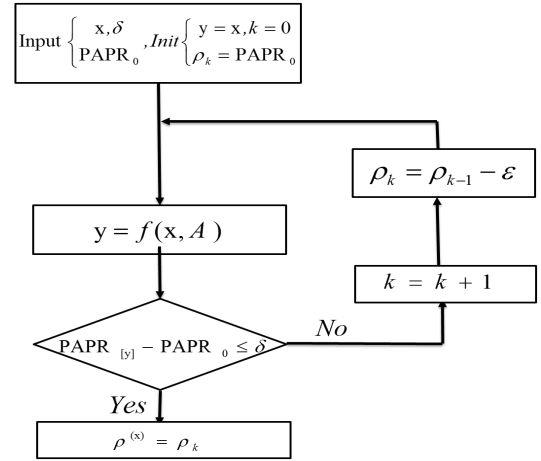


Figure 4. Flow chart of the AC method.

of the ideal clipping depicted in Fig. 1. Fig. 5 depicts the PAPR values ($PAPR_{[y]}$) obtained after a PAPR reduction carried out by means of the AC and CC method, versus their PAPR values before clipping (the initial PAPR values).

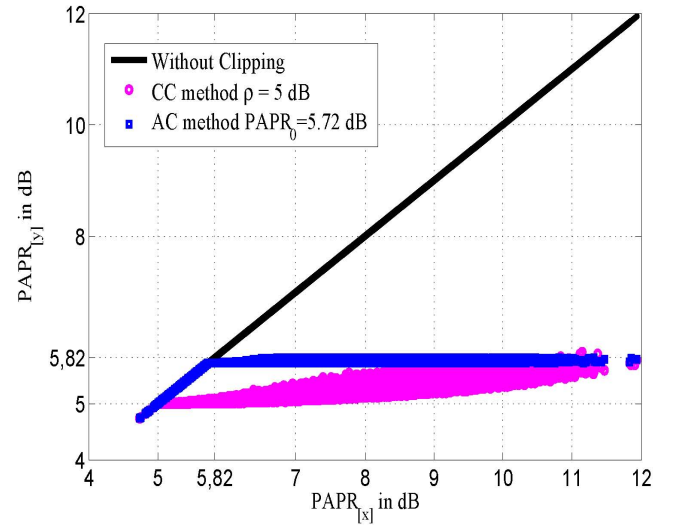


Figure 5. PAPR values after a PAPR reduction obtained by means of the AC and CC methods for OFDM symbols, versus the associated PAPR value before PAPR reduction. $M = 64$, $L = 4$, $\rho = 5$ dB and $PAPR_0 = \gamma_4(\rho) = 5.82$ dB.

The simulation results depicted in Fig. 5 confirm that in the AC method the output PAPR value of each clipped symbol, i.e., $PAPR_{[y]}$ is approximately equal to the desired output PAPR value, i.e., $PAPR_0$. Therefore, where $PAPR_0 = \gamma_4(\rho)$, the AC method allows us to prevent from clipping the symbol unnecessarily or more severely than necessary as it is the case where the CC method is used. In fact, from Fig. 5, we remark that the symbols, which feature an initial PAPR value that is included in $[5, 5.82]$ (in dB), are unnecessarily clipped. We can also note that those featuring an initial PAPR value greater than 5.82 dB are severely clipped with respect to the obtained useful PAPR value that is $\gamma_4(\rho) = 5.82$ dB, i.e., the

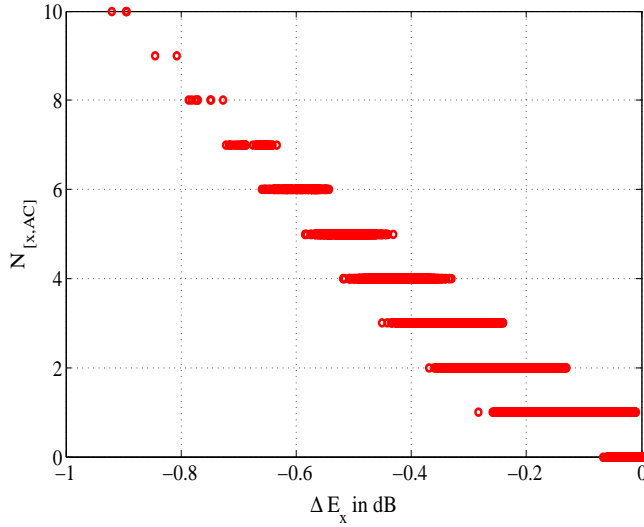


Figure 6. Number of iterations performed by the AC method so as to approach ρ^x , versus ΔE_x . $M = 64$, $L = 4$, $\rho = 3.5$ dB and $\text{PAPR}_0 = \gamma_4(\rho) = 4.62$ dB.

upper bounded PAPR at a CCDF clip that is close to zero (here 10^{-4}). Therefore, the AC will degrade less the OFDM symbol obtained by means of clipping than the CC method and offers similar performances in terms of PAPR reduction. Further simulation pertaining to this aspect will be presented in Section IV.

Since the adaptive threshold has to be computed the AC method is very complex compared to the CC method. From Fig. 4, it can be noticed that, at each iteration, a CC operation is required. Thus, in what follows, the convergence spread, i.e., the mean of number of iterations required so as to find the adaptive threshold of each OFDM symbol, will be discussed. To this end, let us consider $N_{[x,AC]}$ the number of performed iterations that is needed in order to find the adaptive threshold of the OFDM symbol \mathbf{x} . For each \mathbf{x} , let us consider ΔE_x as the mean power variation after PAPR reduction using the CC method or proposed clipping method, and that is defined as follows

$$\Delta E_x = 10 \log_{10} \left(\frac{P_y}{P_x} \right) \quad (10)$$

Fig. 6 depicts the number of iterations performed by the AC method, so as to come close ρ^x versus the value of ΔE_x .

The results depicted in Fig. 6 show that the number of iterations performed so as to find the adaptive of each OFDM symbol depends on its content (ΔE_x). In fact, for each OFDM symbol \mathbf{x} , it can be noted that when ΔE_x increases, the number of iterations that are required to find ρ^x increases significantly and the contrary is also true.

B. Comprehensive search carried out by mean a non constant step (IAC method)

In this section, we present the IAC method, and the theoretical analysis of its performances in terms of PAPR reduction and convergence spread (number of required iterations to find the $\rho^{(\rho)}$). The theoretical comparison with AC, as regards the convergence speed, will be also presented.

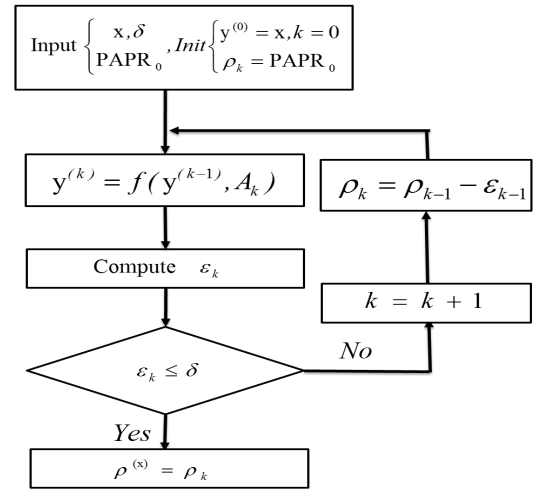


Figure 7. Flow chart of the IAC approach.

Since $\delta > 0$ and since there exist an OFDM symbol \mathbf{x} featuring a PAPR value greater than PAPR_0 , the IAC approach consists of searching the adaptive threshold $\rho^{(\mathbf{x})}$, which satisfies (9). In order to find this threshold we check successively $\rho_0 = \text{PAPR}_0$, $\rho_1 = \rho_0 - \epsilon_1, \dots, \rho_m = \rho_{m-1} - \epsilon_m$ where ϵ_m is the step that allows us to go from stage $m-1$ to the stage m . In contrast to the work presented in [2], the step ϵ_m is not constant and depends on the content of each OFDM symbol and its clipped version at the previous iteration. To this end, we denote $\mathbf{y}^{(m)}$ where $m = 1, 2, \dots$, as being the clipped OFDM symbol featuring the threshold ρ_m , and the step ϵ_m at the m^{th} iteration is expressed as follows

$$\epsilon_m = 10 \log_{10} \left(\frac{P_{\mathbf{y}^{(m-2)}}}{P_{\mathbf{y}^{(m-1)}}} \right), \quad (11)$$

with the notation $P_{\mathbf{y}^{(-1)}} = P_x$ at the first iteration. The flow chart of the adaptive threshold $\rho^{(\mathbf{x})}$ search in the IAC approach is depicted in Fig. 7.

The clipping level magnitude A_m at the m^{th} iteration can be expressed, from the normalized threshold ρ_m , as

$$\begin{aligned} A_m &= 10^{\frac{\rho_m}{20}} \sqrt{P_x} \\ &= \left(10^{\frac{\rho_0 - \epsilon_1 - \dots - \epsilon_m}{20}} \right) \sqrt{P_x} \\ &= \left(10^{\frac{\text{PAPR}_0}{20}} \right) \left(10^{\frac{-\sum_{l=1}^m \epsilon_l}{20}} \right) \sqrt{P_x} \\ &= \left(10^{\frac{\text{PAPR}_0}{20}} \right) \left(\prod_{l=1}^m 10^{\frac{-\epsilon_l}{20}} \right) \sqrt{P_x}. \end{aligned} \quad (12)$$

Then, from (11) we obtain after some derivation the following

expression of the clipping magnitude at the m -th iteration A_m

$$\begin{aligned} A_m &= \left(10^{\frac{PAPR_0}{20}}\right) \left(\prod_{l=1}^m \sqrt{\frac{P_{\mathbf{y}}^{(l-1)}}{P_{\mathbf{y}}^{(l-2)}}}\right) \sqrt{P_{\mathbf{y}}} \\ &= \left(10^{\frac{PAPR_0}{20}}\right) \sqrt{P_{\mathbf{y}}^{(m-1)}}. \end{aligned} \quad (13)$$

Therefore, by substituting (13) in (6) the PAPR of the clipped signal at the m th iteration satisfies the following expression

$$PAPR_{[\mathbf{y}^{(m)}]} - PAPR_0 = \epsilon_{m+1}. \quad (14)$$

If we define $\epsilon_{m+1} \leq \delta$ as the criteria for stopping the IAC method at the m th iteration, then, for each OFDM symbol, the PAPR value of the signal, after PAPR reduction by IAC, is less than $PAPR_0 + \delta$. Thus, the CCDF curve of the IAC will approach the ideal clipping CCDF. Therefore, the IAC method allows us to get the desired deterministic upper bounded PAPR.

From (13) we remark that, as it is noticed in the introduction, the IAC method is equivalent to clipping the signal iteratively, via an adaptation of the clipping magnitude according to $PAPR_0$ and the content of the clipped signal at the previous iteration. The following Algorithm 1 describes the proposed IAC technique.

Algorithm 1 the IAC algorithm

Require: \mathbf{x} input OFDM signal, $\delta > 0$ and $PAPR_0$

Ensure: \mathbf{y}_n output signal

$m \leftarrow 0$

$\epsilon_m \leftarrow 1$

$\mathbf{y}^{(-1)} \leftarrow \mathbf{x}$

while $(PAPR_{\mathbf{y}^{(m)}} - PAPR_0) = \epsilon_m \geq \delta$ **do**

$m \leftarrow m + 1$

Compute A_m from equation (13)

$\mathbf{y}^{(m)} \leftarrow f(\mathbf{y}^{(m-1)}, A_m)$

end while

Fig. 8 depicts $PAPR_{[\mathbf{y}]}$ versus $PAPR_{[\mathbf{x}]}$, where $PAPR_{[\mathbf{y}]}$ is the PAPR value after a PAPR reduction performed by means of the IAC and the CC methods.

On the basis of the simulation results depicted in Figs .8, we remark that, similarly to the AC method, the output PAPR value of each clipped symbol, i.e., $PAPR_{[\mathbf{y}]}$, in the IAC method, is approximately equal to the desired output PAPR value $PAPR_0$, as it is the case in the AC method. Therefore, when $PAPR_0 = \gamma_4(\rho)$, the IAC method prevents us from clipping the symbol unnecessarily or more severely than necessary as it is the case in CC method. Therefore, the IAC method will degrade less the OFDM symbol after clipping than the CC method, and offers same performances in terms of PAPR reduction. More simulation pertaining to this aspect will be presented in Section IV.

In Fig. 9 the number of iterations performed by the IAC method, so as to reach $\rho^{\mathbf{x}}$, versus $\Delta E_{\mathbf{x}}$ is presented. The simulation results show that the IAC method allows a quicker convergence $\rho^{\mathbf{x}}$, in comparison with the AC method (see Fig. 9). Besides, in the IAC method, it can be noticed that the number of required iterations does not increase significantly when $\Delta E_{\mathbf{x}}$ increases.

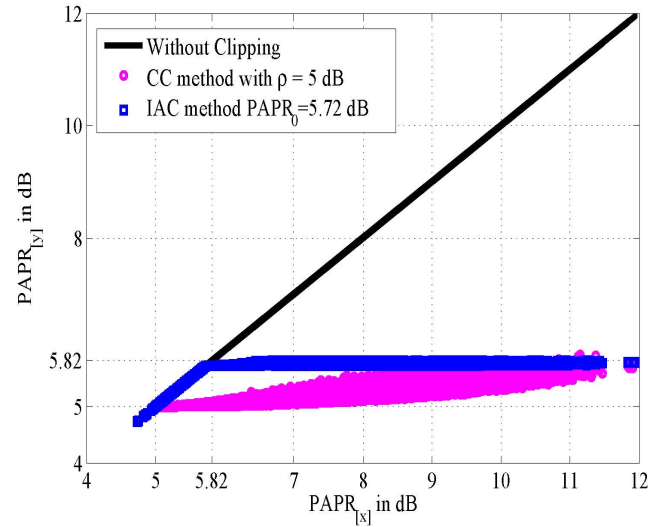


Figure 8. PAPR value obtained after the PAPR reduction of an OFDMs symbols, and performed thanks to the IAC and CC methods, versus the associated PAPR value before PAPR reduction. $M = 64$, $L = 4$, $\rho = 5$ dB and $PAPR_0 = \gamma_4(\rho) = 5.82$ dB

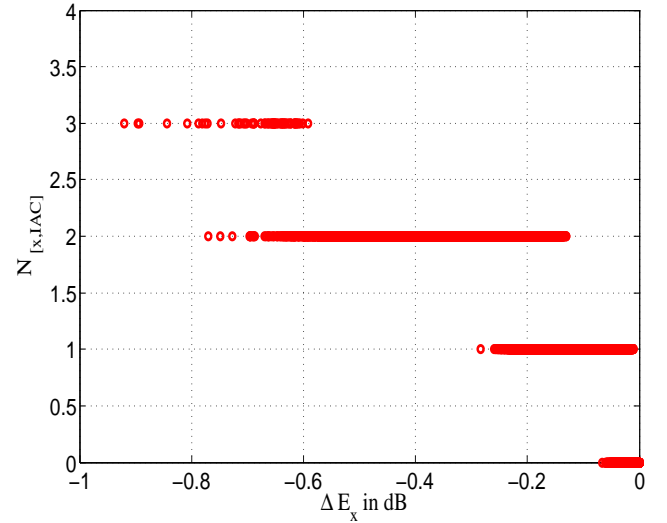


Figure 9. Number of performed iterations by the IAC method so as to find \mathbf{x} , versus $\Delta E_{\mathbf{x}}$. $M = 64$, $L = 4$, $\rho = 3.5$ dB and $PAPR_0 = \gamma_4(\rho) = 4.62$ dB

In what follows, a comparison of the theoretical convergence speeds obtained for the AC and IAC methods will be done thanks to the mean numbers of iterations that are performed by these algorithms for each OFDM symbol.

For each OFDM symbol \mathbf{x} and $\epsilon > 0$, let us consider $N_{[\mathbf{x},AC]}$, $N_{[\mathbf{x},IAC]}$ the number of iterations performed by AC and IAC, respectively, so as to reach $\rho^{(\mathbf{x})}$, subject to the condition in (9). Therefore, $\rho^{(\mathbf{x})}$ is approximated by $\rho_{N_{[\mathbf{x},AC]}} = PAPR_0 - N_{[\mathbf{x},AC]}\epsilon$ and $\rho_{N_{[\mathbf{x},IAC]}} = PAPR_0 - \sum_{l=1}^{N_{[\mathbf{x},IAC]}-1} \epsilon_l$ for AC and IAC, respectively. Let us define the average step used in IAC

to find $\rho_{[N_{x_n, IAC}]}$ as

$$\epsilon_x = \frac{1}{N_{[x, IAC]} - 1} \sum_{l=1}^{N_{x,2}-1} \epsilon_l. \quad (15)$$

Proposition 3.1: For each OFDM symbol \mathbf{x} , we need to find the value of $\rho_{N_{[x_n, IAC]}}$ that depends on the number of iterations performed by AC, and the used step ϵ_x .

To prove this statement (see the proof details in Appendix(A)), it is sufficient to show that the AC method performs $N_{[x_n, IAC]}$ iterations, so as to find the $\rho_{N_{x, AC}}$, where the used step is $\epsilon = \epsilon_x$. In other words, it is sufficient to show that $N_{[x_n, IAC]} = N_{[x_n, AC]}$ when $\epsilon = \epsilon_x$.

Thus, for each OFDM symbol, the comparison between $N_{[x, AC]}$ and $N_{[x, IAC]}$ can be made by means of a comparison between ϵ_x and ϵ . Since \mathbf{x} is random, we will compare IAC and AC, in terms of convergence spread, on the basis of the average number of iterations required by each algorithms, which is equivalent to compare $\mathbb{E}[\epsilon_x]$, as defined in (16), with ϵ (the constant step in AC).

$$\mathbb{E}[\epsilon_x] \simeq \frac{1}{P_x} \sum_{m=0}^{N_2} \int_0^{+\infty} f(r, A_m) p(r) dr \quad (16)$$

where $p(r)$ is the probability density function of the OFDM signal's amplitudes. Please note that N_{IAC} (respectively N_{AC}) represents the average number of iterations performed by the IAC (respectively AC) method, which is estimated thanks to the Monte Carlo trial. After some computations [17], we obtain

$$\mathbb{E}[\epsilon_x] = \frac{1}{P_x} \sum_{m=0}^{N_2} \left(1 - e^{-\frac{A_m^2}{P_x}} \right) \quad (17)$$

Since, in the IAC method, the stopping criterion is $\epsilon_m < \epsilon$ (see Algorithm 1), the comparison between $\mathbb{E}[\epsilon_x]$ and ϵ can be achieved by comparing $\mathbb{E}[\epsilon_1]$ (the first step in IAC method) with ϵ . Therefore, we can deduce that, for each $PAPR_0$ $N_{AC} \geq N_{IAC}$ if and only if

$$\epsilon_1 = 10 \log_{10} \left(\frac{1}{1 - e^{-PAPR_0}} \right) \geq \epsilon.$$

After some derivations, we can conclude that:

$$N_{AC} \geq N_{IAC} \text{ If and only if } PAPR_0 \leq \ln \left(\frac{10^{\frac{\epsilon}{10}}}{10^{\frac{\epsilon}{10}} - 1} \right) \quad (18)$$

Figs. 10 and 11, compare respectively N_{IAC} with N_{AC} and $\mathbb{E}[\epsilon_x]$ with $\epsilon = 0.1$ dB.

The simulation results depicted in Figs. 10 and 11 confirm that comparing N_{IAC} with N_{AC} is equivalent to compare $\mathbb{E}[\epsilon_x]$ with ϵ . In fact, we note that where $N_{AC} \geq N_{IAC} \Leftrightarrow \mathbb{E}[\epsilon_x] \geq \epsilon$. Besides, it is worth noticing that the IAC method converges more rapidly than the AC method when $PAPR_0 \leq 6$, which is consistent with equation (18) (with $\epsilon = 0.1$ dB $\Rightarrow 10 \log_{10} \left[\log \left(\frac{10^{\frac{0.1}{10}}}{10^{\frac{0.1}{10}} - 1} \right) \right] = 5.77$ dB $\simeq 6$ dB).

The AC and IAC methods give both an approximation of the adaptive threshold ρ^* , via respectively an exhaustive search featuring a constant and a non constant step. In this paper, we propose a new approach that allows to find the exact solution of (8). This approach is based on an approximation of the mean power P_y and is presented in the Section III-C.

C. Mean power approximation based approach: the PAC method

In this section, a new approach to compute the adaptive threshold ρ^* is presented. This approach consists of using an approximation of the mean power P_y , see (8), to compute ρ^* . Thus, it will be named PAC (Power approximation based approach for AC).

Let us consider $A^{(x)}$ the clipping magnitude obtained from the normalized adaptive threshold $\rho^{(x)}$, i.e.,

$$A^{(x)} = \sqrt{P_x} \left(10^{\frac{\rho^{(x)}}{20}} \right) \quad (19)$$

From (8), it can be easily remarked that $0 \leq \rho^{(x)} \leq PAPR_0$, therefore,

$$A_0 \leq A^{(x)} \leq A_1 \quad (20)$$

where

$$\begin{aligned} A_0 &= \sqrt{P_x} \\ A_1 &= \sqrt{P_x} \left(10^{\frac{PAPR_0}{20}} \right) \end{aligned} \quad (21)$$

For each clipping magnitude A , let us consider $\mathcal{I}(A)$ the set comprising the index of the \mathbf{x} values, which exceed the clipping magnitude A , i.e.,

$$\mathcal{I}(A) = \{l, \text{ such that } |x_l| > A\} \quad (22)$$

Therefore, from (20) we have

$$\mathcal{I}(A_1) \subset \mathcal{I}(A^{(x)}) \subset \mathcal{I}(A_0), \quad (23)$$

Since the value of $\mathcal{I}(A^{(x)})$ is known, (8) can be expressed as a function of the unknown value $A^{(x)}$ as follows

$$PAPR_0 \underbrace{\left(\sum_{l \notin \mathcal{I}(A^{(x)})} \frac{|x_l|^2}{LM} + \frac{\text{Cardinal}(\mathcal{I}(A^{(x)}))}{LM} (A^{(x)})^2 \right)}_{P_y} = (A^{(x)})^2 \quad (24)$$

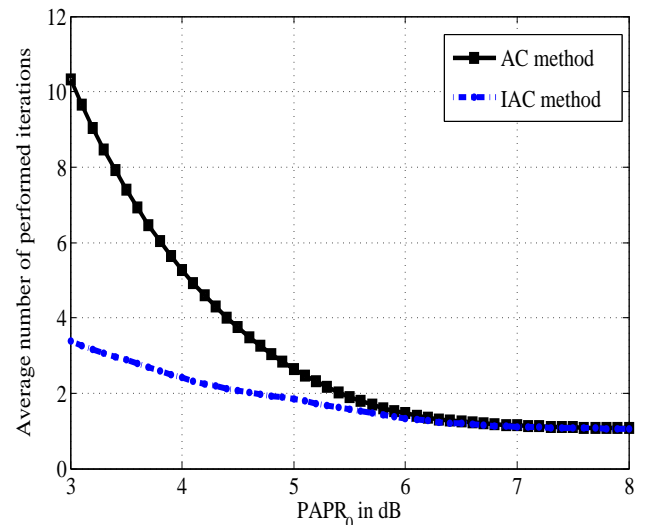
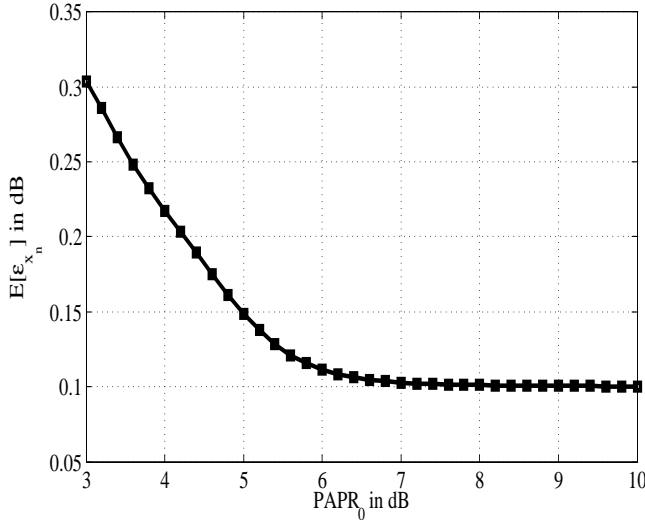


Figure 10. Mean of number of iterations performed by IAC and AC for each OFDM symbol, versus $PAPR_0$


 Figure 11. Comparison between $\mathbb{E}[\epsilon_x]$ and $\epsilon = 0.1$ dB, versus PAPR_0

It can be noted from (24), that if $\mathcal{I}(A^{(\mathbf{x})})$ is known, then the mean power of the clipped symbol that uses, i.e., P_y , can be expressed explicitly as a function of \mathbf{x} and $A^{(\mathbf{x})}$. Therefore, the suitable clipping magnitude can be computed thanks to (24). Thus, using (23), the PAC method comprises two stages:

Stage 1: Computation of $\mathcal{I}(A^{(\mathbf{x})})$.

Since A_0 and A_1 have been determined, the goal consists of finding A_{min} and A_{max} via a dichotomy search method so that:

$$\left\{ \begin{array}{l} A_{min} \leq A \leq A_{max} \\ \mathcal{I}(A_{min}) = \mathcal{I}(A^{(\mathbf{x})}) = \mathcal{I}(A_{max}) \\ \#\mathcal{I}(A_{min}) = \#\mathcal{I}(A^{(\mathbf{x})}) = \#\mathcal{I}(A_{max}) \end{array} \right. \quad (25)$$

Graphically, as A_0 and A_1 are known, the dichotomy search allows us to move from the configuration shown in Fig. 12 to the configuration shown in Fig. 13.

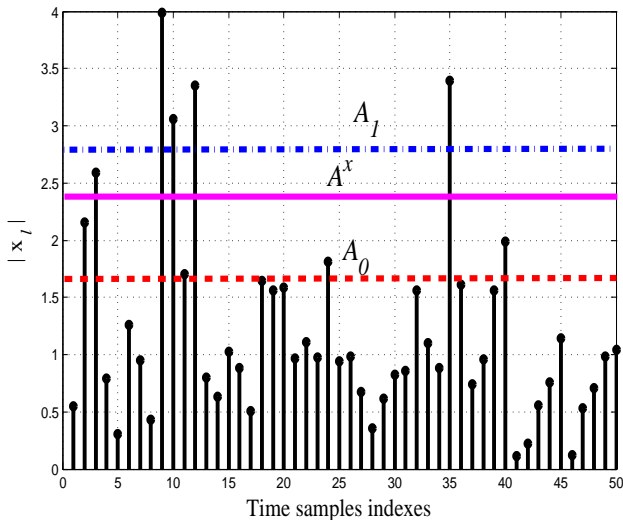


Figure 12. Initial configuration stage.

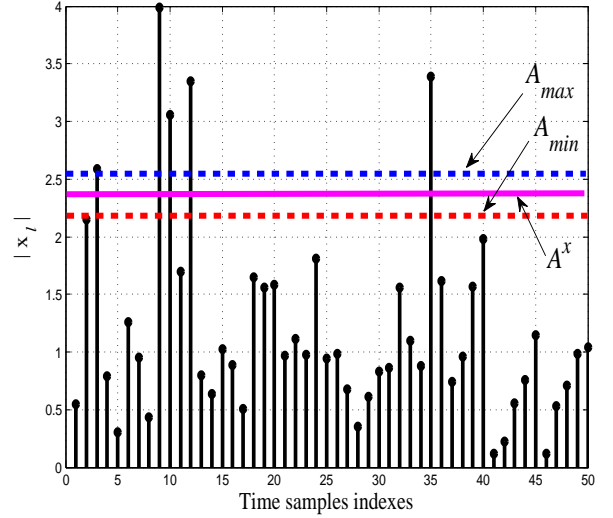


Figure 13. Final configuration stage.

From Fig. 13, we remark that $\mathcal{I}(A^{(\mathbf{x})})$ can be found without knowing $A^{(\mathbf{x})}$.

Stage 2: Computation of $A^{(\rho)}$ by solving (24).

Since $\mathcal{I}(A^{(\mathbf{x})})$ has been determined, this stage consists of solving (24). After some derivations, it can be shown that

$$A^{(\mathbf{x})} = \sqrt{\frac{\frac{\text{PAPR}_0}{LM} \sum_{l \notin \mathcal{I}(A^{(\mathbf{x})})} |x_l|^2}{1 - \text{PAPR}_0 \frac{\text{Cardinal}(\mathcal{I}(A^{(\mathbf{x})}))}{LM}}} \quad (26)$$

After a dichotomy search method, the computation of the set $\mathcal{I}(A^{(\mathbf{x})})$ is described in detail in Fig. 14.

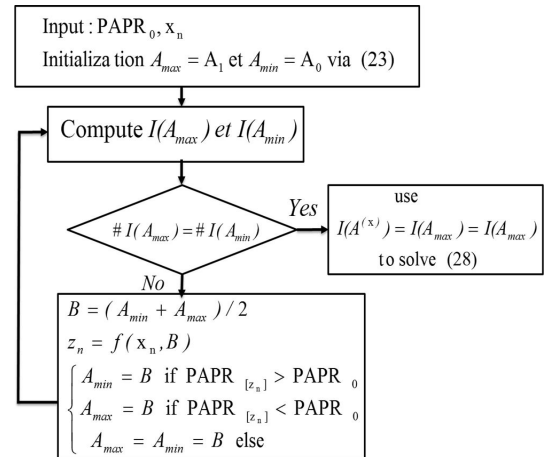

 Figure 14. Flow chart of the PAC approach used to find $\mathcal{I}(A^{(\mathbf{x})})$.

Fig. 15 depicts $\text{PAPR}_{[y]}$ versus $\text{PAPR}_{[x]}$, where $\text{PAPR}_{[y]}$ denotes the output PAPR value obtained after a clipping process that uses the PAC and CC methods.

As in previous analysis related to the AC and IAC methods, it can be noticed that the PAC method allows us to prevent the unnecessarily clipping or the more severely than necessary

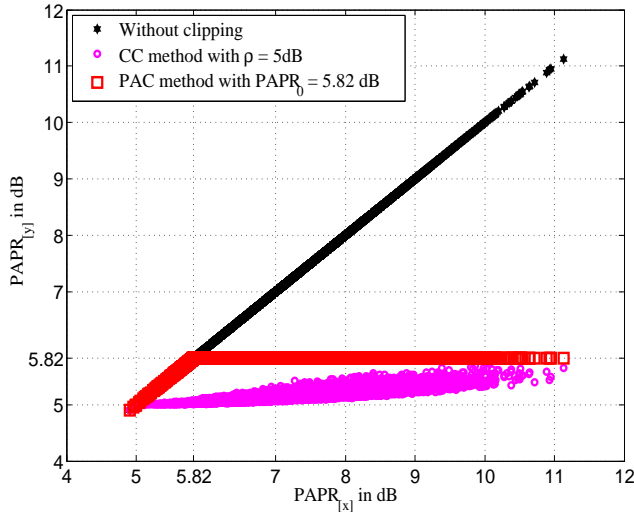


Figure 15. PAPR value after a PAPR reduction of an OFDMs symbols, by means of the PAC and CC methods, versus its PAPR value before PAPR reduction. $M = 64$, $L = 4$, $\rho = 5$ dB and $\text{PAPR}_0 = \gamma_4(\rho) = 5.82$ dB.

clipping, for each OFDM symbol where $\text{PAPR}_0 = \gamma_4(\rho)$ (see Fig 15). In fact, we note that, when the CC method is used, the symbols whose initial PAPR value is included in $[5, 5.82]$ (in dB) are unnecessarily clipped and those with an initial PAPR value is greater than 5.82 dB are severely clipped with respect to the obtained useful PAPR value $\gamma_4(\rho) = 5.82$ dB (i.e., the upper bounded PAPR of the CCDF at a clip rate that is close to zero (here 10^{-4})). Therefore, the PAC method will degrade less the OFDM symbols after the clipping than the CC method for the same PAPR reduction performances. Besides, unlike the AC and IAC methods, the PAPR value of each clipped symbol, in the PAC method, is exactly equal to $\text{PAPR}_0 = \gamma_4(\rho)$. More simulation results will be presented in Section IV. As in the previous section, we will evaluate, in what follows, the number of required iteration so as to find $A^{(x)}$. To this end, for each OFDM symbol x , let us consider $N_{[x, \text{PAC}]}$ the number of performed iterations so as to find $A^{(x)}$.

Fig. 16 depicts the number of iterations performed by the AC method in order to approach ρ^x versus ΔE_x . Obtained results depicted in Fig. 16 show that the number of iterations performed, so as to find the adaptive threshold of each OFDM symbol does not depend on ΔE_x . In fact, the curve depicting the number of iterations in function of ΔE_x is not monotonic. On the basis of the simulation results depicted in Figs. 6 and 9, it appears that this approach requires generally more iterations than the AC and IAC approaches. In Section IV, the previous approaches and the PAC method will be compared as regards the average number of required iterations versus PAPR_0 . In other words, we will compare $\mathbb{E}[N_{[x, \text{AC}]}]$, $\mathbb{E}[N_{[x, \text{IAC}]}]$ and $\mathbb{E}[N_{[x, \text{PAC}]}]$ where $\mathbb{E}[\cdot]$ is the expectation. The Monte Carlo method will be used for this estimation.

IV. SIMULATION RESULTS

As in the previous section, the performance of the proposed AC, IAC and PAC methods versus that of the CC method are analysed within the framework of a specific PAPR reduction. In other words, if the CC method is performed by means of

the predefined normalized threshold ρ , the AC, IAC and PAC will be performed using and $\text{PAPR}_0 = \gamma_4(\rho)$ and $\text{PAPR}_0 = \gamma_4(\rho) - \epsilon$, where $\gamma_4(\rho)$ denotes the PAPR achieved via the CC method. Note that, $\gamma_4(\rho)$ is the upper bounded PAPR for a 10^{74} value. The simulations are performed for an OFDM signal featuring 16-QAM modulation, $M = 64$ and an oversampling factor $L = 4$.

Figs. 17 and 18, with $\rho = 3.5$ dB and 5 dB, respectively, confirm that the CCDF curves of the AC, IAC and PAC approximate the ideal clipping CCDF curve. Besides, the proposed AC methods and the CC method achieve the same upper bounded PAPR value for a CCDF curves clip rate equal to 10^{-4} . It is worth noting that given the depicted results the AC, IAC and PAC methods reach a deterministic upper bounded PAPR. In the following, the AC, IAC and PAC methods are compared with the CC method as regards the BER degradation.

The results depicted in Figs. 19 and 20 show that the AC, IAC, and PAC methods outperform the CC method in terms of BER degradation. The gain obtained for a BER of 10^{-4} , is approximately equal to 0.5 dB in Fig. 20 and 3 dB in Fig. 19. These results confirm the theoretical analysis undertaken in Sections III-A, III-B and III-C, where the authors have shown that, where the CC method is used many OFDM symbols are clipped more severely (see AREA 2 in Fig. 3) than necessary or clipped unnecessarily (see AREA 1 in Fig. 3) with respect to γ_4 .

The mean power degradation and the adjacent channels pollution, which is due to the effect of the OOB components, are depicted in Fig. 21 and Fig. 22.

From the simulation results depicted in Fig. 21, it can be noticed that the AC, IAC, and PAC methods decrease less the mean power of the OFDM symbol after a PAPR reduction than the CC method featuring the same achieved PAPR for a CCDF's clip rate equal to 10^{-4} . For example, where $\gamma_4 = 4.72$ dB, $\Delta E = -0.47$ dB in CC method and

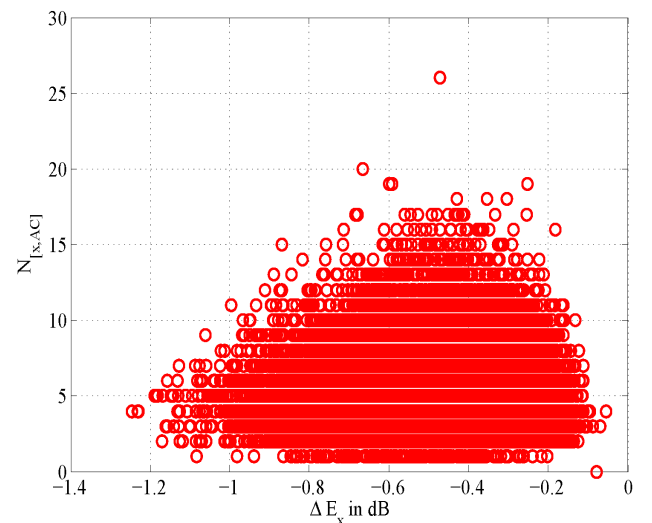


Figure 16. Number of iterations performed by the PAC method so as to find $A^{(x)}$ versus ΔE_x . $M = 64$, $L = 4$, $\rho = 3.5$ dB and $\text{PAPR}_0 = \gamma_4(\rho) = 4.62$ dB.

$\Delta E = -0.25$ dB in the proposed AC methods.

Fig. 22 depicts the Power Spectrum Density (PSD) of the OFDM signal before and after PAPR reduction where using the proposed AC method and the CC method.

Besides the achieved BER performance in Figs. 19, 20, and attained mean power variation in Fig. 21, it can be noted from Fig. 22 that the proposed AC methods are less polluting than the CC method when $\text{PAPR}_0 = \gamma_4 - \epsilon$, i.e., for the same PAPR value. As a general conclusion, the obtained results pertaining to mean power degradation, Out-Of-Band emission and BER degradations confirm that where $\text{PAPR}_0 = \gamma_4 - \epsilon$, i.e., within the framework of a similar achieved output PAPR, the AC, IAC and PAC methods induce less degradation than the CC method (see Figs. 19, 20, 21, 22 and 23, which is a zoom of Fig. 22).

In the following, we compare the required average number of iterations performed by the proposed AC method so as to find the adaptive threshold of each OFDM symbol that we want to clip. Fig. 24 shows that IAC method converges more quickly than AC and PAC methods. The simulation results show also that the PAC method required more iterations than the AC and IAC methods so as to find the suitable bound of the adaptive magnitude clipping $A^{(\times)}$. However, it is important to note that the PAC method gives an exact solution of (8) whereas the AC and IAC give an approximation of the solution. Besides, it can be remarked that $N_1 \geq N_2$ when $\gamma_4 \leq 6$, which is coherent with equation (18) (with $\epsilon = 0.1$ dB \Rightarrow $10 \log_{10} \left[\log \left(\frac{10^{\frac{0.1}{10}}}{10^{\frac{0.1}{10}} - 1} \right) \right] = 5.77$ dB \simeq 6 dB).

V. CONCLUSION

In this paper, a new clipping method is presented. In the latter, each OFDM symbol is clipped with respect to the desired output upper bounded PAPR_0 , which is obtained thanks to an adaptive threshold. Three methods (AC, IAC, and PAC) are proposed for the computation of the adaptive threshold. The theoretical analysis and simulation results achieved in

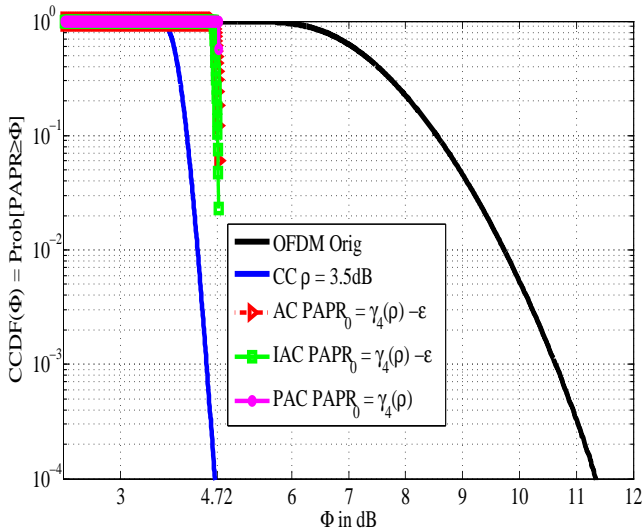


Figure 17. CCDF curves before and after PAPR reduction where using the CC, AC, IAC and PAC methods, and with $\rho = 3.5$ dB.

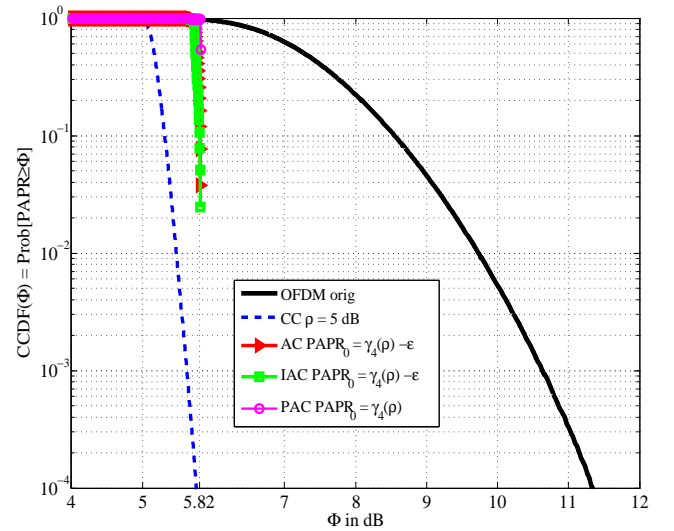


Figure 18. the CCDF curves before and after PAPR reduction where using the CC, AC, IAC and PAC methods, and with $\rho = 5$ dB.

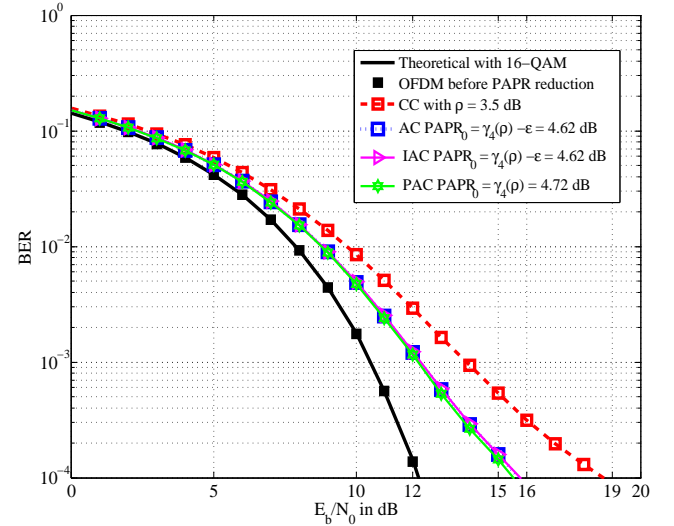


Figure 19. Comparison between the CC method and proposed AC methods, in terms of BER degradation, and with $\rho = 3.5$ dB.

this paper show that the adaptive threshold can be efficiently computed by means of the IAC method. This approach converges more quickly than the one based on exhaustive research featuring a constant step and than the PAC method. However, the PAC method allows finding the exact adaptive threshold for each OFDM symbol. Thanks to these approaches, the proposed AC method achieves the best performances whatever the method to compute the threshold is, and offers similar performances in terms of PAPR reduction. Furthermore, the proposed AC method gives a deterministic desired upper bounded PAPR, which is very important for the IBO definition in the case of high power amplifiers (HPA). Our future work will focus on the extension of the proposed work to other clipping functions such as deep clipping and smooth clipping, combined with Out Of Band noise suppression approaches.

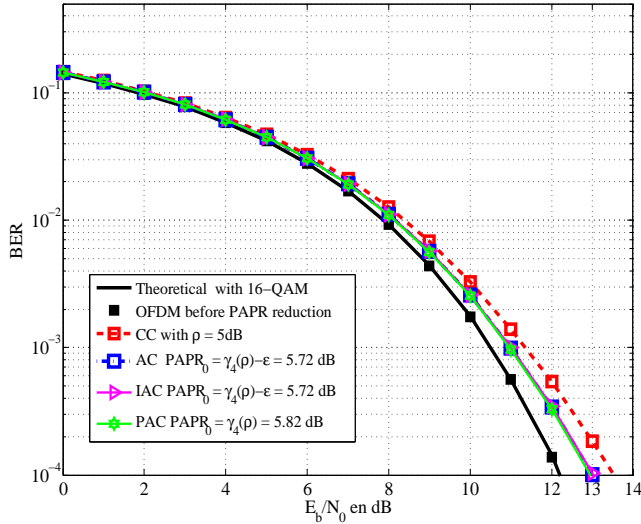


Figure 20. Comparison between the CC method and the proposed AC methods, in terms of BER degradation, and with $\rho = 5$ dB.

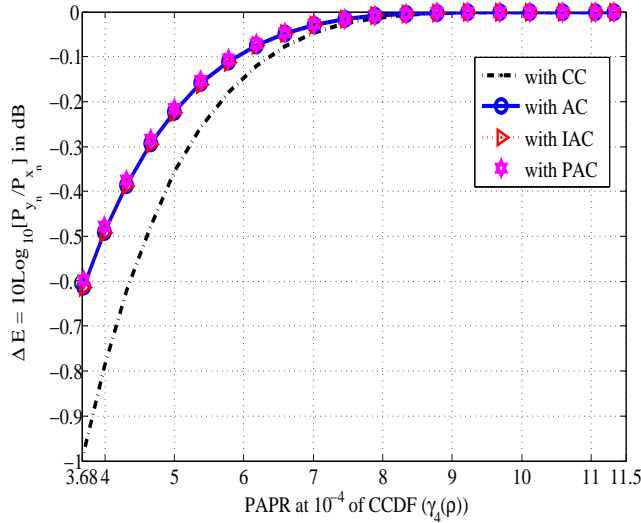


Figure 21. Comparison between the CC method and the proposed AC methods, in terms of Mean Power degradation versus the achieved PAPR for a rate 10^{-4} .

APPENDIX A

PAPR VALUE OF THE CLIPPED OFDM SYMBOL USING THE THRESHOLD ρ_m IN THE AC METHOD

Proof: In this section, we detail the proof related to (15). Therefore, let ρ_m , $m = 1, 2, \dots$, be the checked step at the m -th iteration (see Fig. 4). Then, from (7), the PAPR value of the clipped OFDM symbol using the threshold ρ_m in the AC method can be expressed as follows

$$\begin{aligned} \text{PAPR}_{[y^{(m)}]} &= \text{PAPR}_0 - (m-1)\epsilon + 10\log_{10}\left(\frac{P_x}{P_{y^m}}\right) \\ &= \text{PAPR}_0 - (m-1)\epsilon_x + 10\log_{10}\left(\frac{P_x}{P_{y^m}}\right). \end{aligned}$$

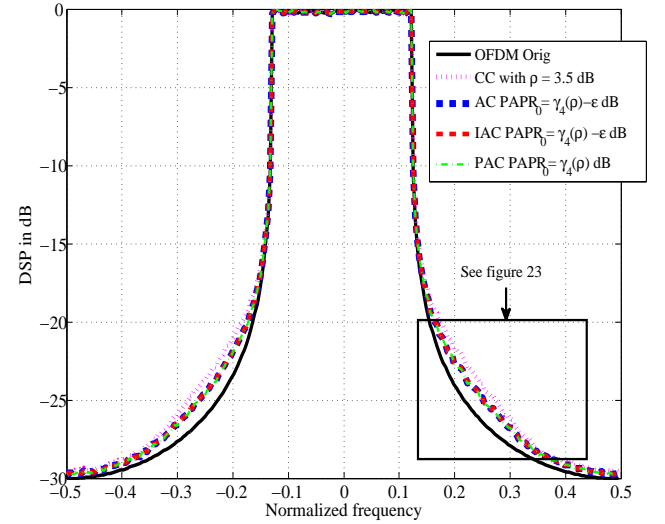


Figure 22. Comparison between PSDs before and after PAPR reduction carried out by means of the proposed methods and the CC method, with $\rho = 3.5$ dB.

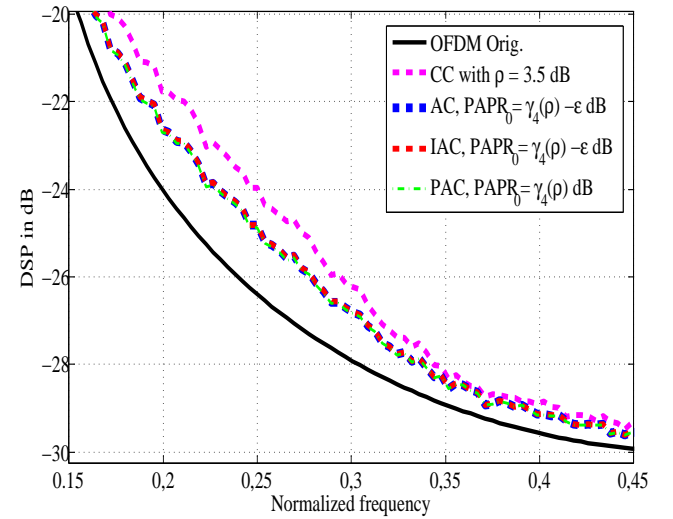


Figure 23. Zoom of Fig. 22. Comparison between the PSD obtained before and after PAPR reduction carried out by means proposed methods and the CC method, with $\rho = 3.5$ dB.

After a few derivations and thanks to (15), we obtain:

$$\text{PAPR}_{[y^{(m)}]} = \text{PAPR}_0 + 10\log_{10} \left(\left[\frac{P_{y^{(N_{[x, IAC]})}}}{P} \right]_{x}^{\frac{m-1}{N_{[x, IAC]}-1}} \frac{P_x}{P_{y^{(m)}}} \right)$$

Since the number of iterations performed by IAC, so as to compute the normalized threshold for the OFDM symbol x , is $N_{x,2}$, we note that

$$\begin{cases} (\text{PAPR}_{[y^{(m)}]} - \text{PAPR}_0) \geq 10\log_{10} \left[\frac{P_{y^{(m-1)}}}{P_{y^{(m)}}} \right] \\ \geq \epsilon_m > \epsilon \text{ If } m < N_{[x, IAC]} \\ (\text{PAPR}_{[y^{(m)}]} - \text{PAPR}_0) = \log_{10} \left[\frac{P_{y^{(N_{[x, IAC]}-1)}}}{P_{y^{(N_{[x, IAC]})}} \right] \\ = \epsilon_{N_{x,2}+1} < \epsilon \text{ If } m = N_{[x, IAC]} \end{cases}$$

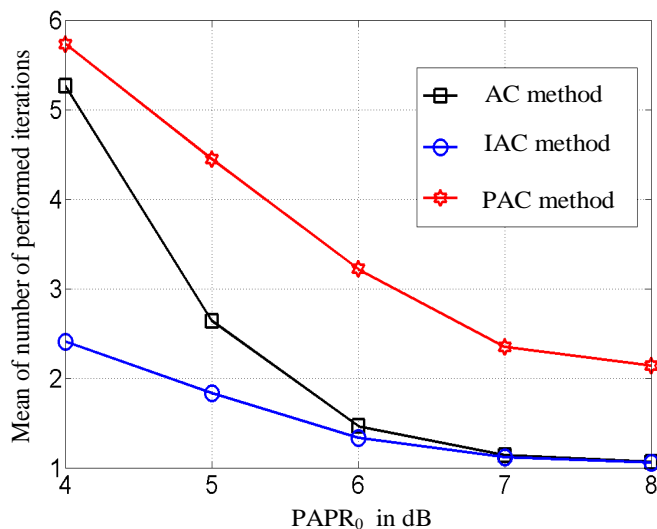


Figure 24. Mean number of iterations performed by IAC and AC for each OFDM symbol in function of PAPR₀.

The latter proves that, for each x , the number of iterations performed by IAC is equal to the number of iterations performed by AC, where the step is equal to ϵ_x .

ACKNOWLEDGMENT

Part of this work is supported by the project ACCENT5 (Advanced Waveforms, MAC Design and Dynamic Radio Resource Allocation for D2D in 5G Wireless Networks) funded by the French national research agency with grant agreement code: ANR-14-CE28-0026-02.

REFERENCES

- [1] M. L. Diallo, J. Palicot, and F. Bader, "Achieving a Desired Upper Bounded PAPR Value Using a Fast Adaptive Clipping Algorithm," *the Eleventh Advanced International Conference on Telecommunication (AICT)*, pp. 1–6, June, 21–26, Brussels, Belgium 2015.
- [2] M. L. Diallo and J. Palicot, "Adaptive clipping for a deterministic PAPR," (invited paper) in *the Proceedings of the International Conference on Telecommunications and Remote Sensing (ICTRS)*, June 2014, Luxembourg.
- [3] G. Wunder, R. Fischer, H. Boche, and S. Litsyn, "The PAPR Problem in OFDM Transmission: New directions for a long-lasting problem," *IEEE Signal Processing Magazine*, pp. 130–140, Oct. 2013.

- [4] R. Bauml, R. F. H. Fischer, and J. Huber, "Reducing the peak-to-average power ratio of multicarrier modulation by selected mapping," *Electronics Letters*, vol. 32, no. 22, pp. 2056–2057, Oct. 1996.
- [5] S. Yoo, S. Yoon, S. Y. Kim, and I. Song, "A novel PAPR reduction scheme for OFDM systems: selective mapping of partial tones (SMOPT)," *Consumer Electronics, IEEE Transactions on*, vol. 52, no. 1, pp. 40–43, Feb. 2006.
- [6] F. Fischer, H. Mauller, W. Bauml, and B. Huber, "OFDM with reduced Peak-to-Average Ratio by multiple signal representation," *Annales des télécommunication*, vol. 52, Oct. 1997.
- [7] P. Varahram, W. Al-Azzo, and B. Ali, "A low complexity partial transmit sequence scheme by use of dummy signals for PAPR reduction in OFDM systems," *Consumer Electronics, IEEE Transactions on*, vol. 56, no. 4, pp. 2416–2420, Nov. 2010.
- [8] J. Tellado-Mourello, "Peak to Average Power Reduction for Multicarrier Modulation," Ph.D. dissertation, Stanford University, 1999.
- [9] C. Ji, S. Fu, and Y. Zhao, "New method for PAPR reduction based on union strategy in OFDM system," *Journal of Electronics (China)*, vol. 31, no. 5, pp. 427–432, 2014. [Online]. Available: <http://dx.doi.org/10.1007/s11767-014-4054-1>
- [10] S. Zabre, J. Palicot, Y. Louet, and C. Lereau, "SOCP Approach for OFDM Peak-to-Average Power Ratio Reduction in the Signal Adding Context," in *Signal Processing and Information Technology, 2006 IEEE International Symposium on*, 2006, pp. 834–839.
- [11] X. Li and L. Cimini, "Effects of clipping and filtering on the performance of OFDM," in *Vehicular Technology Conference, 1997, IEEE 47th*, vol. 3, 1997, pp. 1634–1638.
- [12] S. Kimura, T. Nakamura, M. Saito, and M. Okada, "PAR reduction for OFDM signals based on deep Clipping," in *Communications, Control and Signal Processing, 2008. ISCCSP 2008. 3rd International Symposium on*, 2008, pp. 911–916.
- [13] Y. K. Byuong Moo Lee, "An adaptive clipping and filtering technique for PAPR reduction of OFDM signals," *Circuit, Systems and Signal Processing*, vol. 32, pp. 1335–1349, 2013.
- [14] H. J. Kim, S. C. Cho, H. S. Oh, and J. M. Ahn, "Adaptive clipping technique for reducing PAPR on OFDM systems," in *Vehicular Technology Conference, 2003. VTC 2003-Fall. 2003 IEEE 58th*, vol. 3, Oct. 2003, pp. 1478–1481.
- [15] J. Armstrong, "Peak-to-average power reduction for OFDM by repeated clipping and frequency domain filtering," *Electronics Letters*, vol. 38, no. 5, pp. 246–247, Feb. 2002.
- [16] Y. Louet and J. Palicot, "A Classification of Methods for Efficient Power Amplification of Signals," *Annals of Telecommunications*, vol. 63, pp. 351–368, 2008.
- [17] D. Guel, "Etudes de nouvelles techniques de réduction de facteur de crête à compatibilité descendante pour les systèmes multiporteuses," Ph.D. dissertation, In French, Université de Rennes 1, Nov. 2009.

Radio Resource Allocation for Indoor Secondary Access in TV White Space

Mohamed Hamid

University of Agder
Grimstad, Norway

Email: mohamed.hamid@uia.no

Niclas Björnsell

University of Gävle
Gävle, Sweden

Email: niclas.bjorsell@hig.se

Abstract—This paper considers fair radio resource assignment for secondary users operating in TV white space by means of frequency hopping. The achieved throughput for different secondary users is used to measure the degree of fairness. The permissible transmission power for secondary users is set to protect the TV transmission from excessive interference. Hence, there are different limits on the secondary transmission power when operating in different idle TV channels because different adjacent channels generates different amounts of interference based on the TV receiver transfer function in the frequency domain. Moreover, different free TV channels experience different amounts of interference due to the non-linearities in the TV transmission. A model for power assignment in each of the free TV channels is developed based on the received TV signal, TV receiver characteristics and secondary user location. For the sake of fair resource allocation, frequency hopping is proposed herein, and its performance is evaluated. In this study, three different TV transmitters located in three different cities in Sweden, namely, Gävle, Stockholm and Linköping, are exploited where the interference from the TV transmission into the free channels is measured. For the secondary system, the deployment of indoor WiFi access points in an office environment is considered and simulated. The main finding is that frequency hopping can provide fair radio resource distribution in terms of the obtainable throughput. Moreover, it is shown that the denser the area is, the higher the achievable secondary throughput due to the higher attenuation of the interfering signals.

Keywords—TV white space; Radio Resource Allocation; WiFi Access Points; Secondary Spectrum Access; Frequency Hopping; Throughput; TV Transmission Interference.

I. INTRODUCTION

This paper is an extended version of [1] and it reports more measurements analyses.

At the beginning of its appearance, designers of wireless communication systems designers were concerned about coverage to provide as wide as possible wireless access. Thereafter, capacity concern began to emerge where not only coverage is considered but also data rates as high as needed are pursued [2]. Previous studies realized that the capacity of wireless networks had doubled every two and a half years over a span of 104 years [2]. However, later studies have shown that this rate is currently higher, but for the sake of illustration, we can assume that this rate of wireless throughput increase currently holds, then, we have a one million-fold increase since 1965. This explosive growth is attributed to the reduced cell size and the availability of the spectrum with wider bandwidths [3]. In fact, both factors have their roots in spectrum-related aspects, as the former is feasible with the aid of spectrum reuse. Consequently, a fundamental question that arises is do we have sufficient and wide spectrum to go further with smaller cell

sizes and provide higher data rates for the foreseeable future wireless access traffic demands? The answer to this question might be yes up to now but it will change to no at some point because we can not support infinite increase of this data traffic due to the existence of finite resources. Here, resources preliminary refer to the financial resources, infrastructure and electromagnetic radio spectrum. The concerns regarding the radio spectrum availability to adopt the growth in mobile data traffic has translated into a phenomenon known as spectrum scarcity [4].

Simultaneously with the emerging spectrum scarcity phenomenon, many experimental investigations have determined that the radio spectrum below 6 GHz is inefficiently utilized, where the duty cycles of some wireless systems reaches 1% or less [5]–[7]. Considering both facts of the need for more spectral resources and being inefficient in utilizing the current available spectrum forms a paradox. A framework that makes use of this paradox by accessing the spectrum opportunistically called cognitive radio (CR) was first proposed at [8]. CR enables flexible access to the radio spectrum, which can significantly enhance spectrum utilization efficiency [9]–[11]. Therefore, the ultimate objective of CR is to mitigate the spectrum scarcity by enabling dynamic spectrum access (DSA), which allows unlicensed users, so-called secondary users (SUs), to identify unutilized channels in the licensed spectrum and utilize them dynamically as long as they do not cause unacceptable interference to the communication by the legacy spectrum licensees known as primary users (PUs) in CR and DSA terminologies [12], [13]. The temporarily unused portions of the spectrum are called spectrum white spaces (WS), spectrum holes or spectrum opportunities. Throughout this paper, the term WS will be used, which may exist in time, frequency, and space domains. To find a WS, one of three approaches can be used, namely, spectrum sensing, beacon signal and geo-location database [14]. Both spectrum sensing and beacon signals are beyond the scope of this paper.

Using a geo-location database for accessing spectrum holes was proposed in [15] and has subsequently been extensively used in literature. With a geo-location database approach, the SU needs to reports its location into a database, which then informs the SU about the available spectrum to use with the associated constrains. A geo-location database is potentially beneficial when the activity pattern of the PU is highly predictable or slowly varying (quasi-static) over time. Such systems include the terrestrial TV transmission and the radar systems [16]. With a TV transmitter as a PU, the free of use channels are called TV white space (TVWS).

In the case of terrestrial TV broadcasting, to avoid exces-

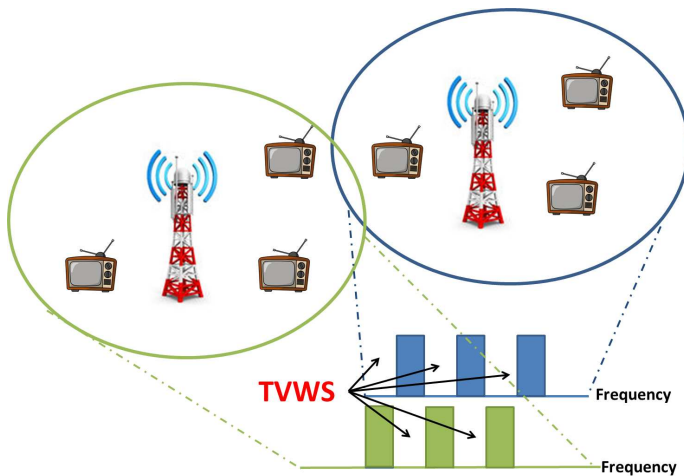


Figure 1. TVWS concept. The free channels located to the right are available for low-power secondary access at the left location and vice versa.

sive interference into the TV transmission, SUs cannot use the same channel. However, interference caused by SUs is not only limited to co-channel interference. In particular, in short-range scenarios, adjacent channel interference is an equally severe problem. In [17], indoor home scenarios with cable, rooftop antenna and set-top antenna reception of TV signals were analyzed. The spectrum reuse opportunities for SUs have been determined using the number of channels where it is possible to transmit without causing harmful interference to TV receivers as a performance measure. Consequently, the transmission capacity depends on which of the free channels are assigned for a specific SU. Free channels that are exposed to interference from either local or neighboring TV masts will have lower throughput. One approach to allocate the available channels in a fair way among the users is to switch channels using a pseudo-random sequence, i.e., using *frequency hopping*.

In the literature, the most related work is reported in [18] and [19]. In [18], the potentials and performance of WiFi-like network deployments in TVWS are studied. In [19], the attainable throughput of WiFi systems deployed in TVWS is studied in comparison to the current deployment approach in the ISM band.

In contrast to the related work in the literature, the distinct contributions of this paper are as follows:

- TV reception protection, TV transmission interference into free channels and the secondary to secondary interference are all considered to provide a full picture for a secondary access scenario.
- A combination of measured data together with simulations are used to obtain a realistic representative environment.
- Frequency hopping is adopted as a technique to fairly distribute the available free channels among the secondary users.
- The interference from the TV transmission into the free channels is empirically evaluated. This interference is because of the non-linearities in the TV transmitter chain in forms of spectrum leakage and intermodulation products.

- The performance of secondary operation in TVWS is evaluated in three different representative locations in Sweden.

The remainder of this paper is structured as follows. Section II introduces the system model, including the TV broadcasting transmission, the sharing model, SU power assignment and the propagation model. In Section III, the motivation for the frequency hopping framework is presented and discussed. The methodology for obtaining the parameters and for the performance evaluation is presented in Section IV. Section V shows the numerical results and interpretations. Finally, Section VI concludes the paper.

II. SYSTEM MODEL

This section addresses aspects related to the system model and is further divided into three subsections. The first subsection overviews the concept of WiFi-like secondary operations in TVWS. The proceeding subsection explains how the maximum allowed transmission power of the APs is executed. Finally, the last subsection shows the model used to determine the received downlink power at the SUs terminals.

A. WiFi Secondary Access to the Terrestrial TV Band

The UHF terrestrial TV broadcasting band lies between 470–862 MHz and is divided into 49 of channels 8 MHz each. 7.6 MHz is used for TV signals within each channel, while 0.4 MHz is deducted and evenly distributed as two guard bands at each side of the channel. The 49 channels are indexed as j , where

$$21 \leq j \leq 49. \quad (1)$$

Each channel j location in the frequency domain is determined as

$$j : 470 + 8 \times (j - 1) \leq 470 + 8 \times j. \quad (2)$$

A single TV transmitter serves a coverage area with a radius of 30 – 50 km using a transmission power of 40 – 50 dBW. Due to the high power of the TV transmitter and high TV masts, neighboring TV transmitters use different broadcasting channels (typically less than 10 channels). Consequently, in each geo-location, a number of TV channels (generally more than 40 channels) exist that are unoccupied and potentially usable for low-power short-range secondary operation. These unoccupied TV channels are called TVWS. Figure 1 presents a conceptual demonstration of TVWS.

According to [20], WiFi-like short-range indoor wireless systems are the 'sweet point' for secondary operations in TVWS for techno-economical considerations. Therefore, the deployment of WiFi access points (APs) is considered in the studies conducted in this paper. It is assumed here that among the unoccupied TV channels, a specific number of channels M is available for the deployed APs. With secondary indoor operation in TVWS, both secondary and TV reception experience interference from TV and secondary transmissions respectively. Figure 2 illustrates the entire system model including mutually interfering signals and geo-location database accessibility. Hereafter, WiFi APs are deployed following the layout shown in Figure 3, where all APs are attached to the

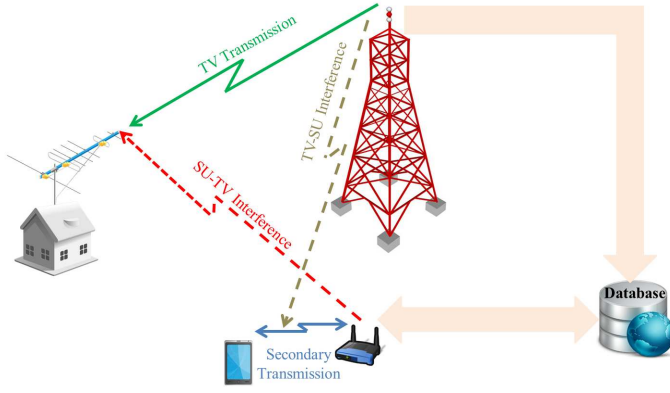


Figure 2. TVWS spectrum sharing using the geo-location database-based spectrum opportunities model. The geo-location database is populated by the TV transmitter either directly or by other entities such as spectrum sensing device or network. SUs access the database to inspect the available radio channels and their associated parameters. SUs also have to report their existence to the database to update different transmission parameters.

building's ceiling and equally spaced. Each SU terminal is linked to the closest AP. Users are uniformly distributed throughout the entire building and within each floor.

B. Permissible Transmission Power of APs

The permissible transmission power model is based on the interference tolerance of adjacent channels of the TV receiver, which guarantees a certain minimum level of TV reception quality. In [21], interference of adjacent channels was experimentally evaluated. The aggregate interference coming from multiple SUs into channel L at specific location coordinates (x, y) is denoted as $I_{tot}(x, y)$, which is calculated as

$$I_{tot}(x, y) = \sum_{k \neq 0} \sum_{j=1}^N I_{j, k+L}(x, y), \quad (3)$$

where (x, y) are evaluated with a reference $(0, 0)$ denoting the TV transmitter mast location, N is the total number of SUs, and $I_{j, k+L}(x, y)$ is the interference injected by the j^{th} SU occupying channel $k + L$ into a TV receiver located at (x, y) .

If the TV received power on channel L at location (x, y) is $S_L(x, y)$ and the minimum acceptable signal-to-interference ratio (SIR) is γ , then to meet the TV reception requirements, we should satisfy

$$S_L(x, y) \geq \gamma + I_{tot}(x, y). \quad (4)$$

where all quantities in (4) are on the logarithmic scale, i.e., dB.

To determine the maximum permissible transmission power on channel $k + L$, one needs to account for the aggregate interference from multiple SUs. Hence, a margin of δ dB can be used to compensate for this adjacent interference. Accordingly, the maximum permissible transmission power for a SU in channel $k + L$ at location (x, y) , say $P_{k+L}^t(x, y)$, is found as

$$P_{k+L}^t(x, y) = S_L(x, y) - \gamma - \zeta(k) - \delta \quad (5)$$

where $\zeta(k)$ is the k^{th} adjacent channel power ratio (ACPR), which represents the difference between the power received

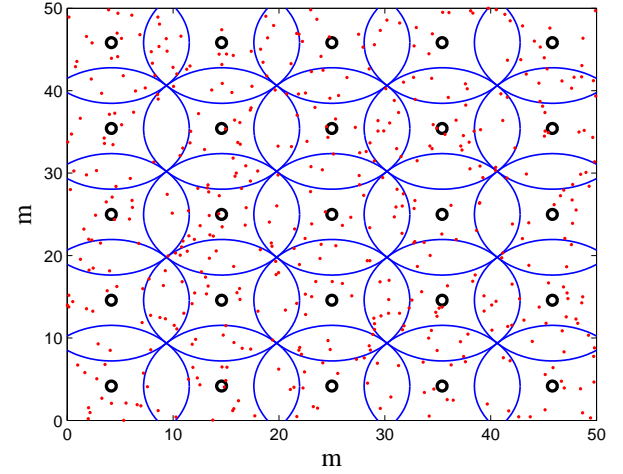


Figure 3. Deployment layout of APs. The APs are the small black rings. The blue circles represent the areas served by the APs to reflect the concept that each SU terminal is attached to its closest AP. The red dots are the users' terminals. Both the x and the y axes represent hypothetical Cartesian coordinates in units of meters.

in a specific channel and the power leaked from the adjacent channel k into that channel. $\zeta(k)$ is dependent on the selectivity curve of the TV receiver, which is determined as

$$\zeta(k) = \left(\int_{f_l^{k+L}}^{f_h^{k+L}} |H(f)|^2 dx \right)_{[dB]} - \left(\int_{f_l^L}^{f_h^L} |H(f)|^2 dx \right)_{[dB]}, \quad (6)$$

where f_l^i and f_h^i denote the upper and lower limits of the i^{th} TV channel, respectively, and $H(f)$ is the TV receiver's transfer function in the frequency domain. Both integration terms of 6 are on their logarithmic scale.

C. Received Power at SU Terminals

To obtain the received power at each SU terminal, a propagation model is required. In [22], a propagation model based on combining the COST 231 [23] model and ITU-R P.1238 [24] is developed. The model calculates the path loss between the SU transmitter and receiver as

$$PL(d, f) = PL_{FS} + \alpha d + n_w L_w + n_f L_f + A, \quad (7)$$

where $PL(d, f)$ is the path loss when the transmitter operates at a frequency of f MHz and located at a distance of d meters from the receiver. n_w , n_f , L_w and L_f are the number of penetrated walls, number of penetrated floors, loss per wall and loss per floor, respectively, α and A are constants. Table I shows the model parameters for the case of an office environment.

To account for the shadow fading, the received power at channel $k + L$ in location (x, y) is denoted as $P_{k+L}^r(x, y)$ and modeled as a log-normally distributed random variable with a mean $(P_{k+L}^t(x, y) - PL(d, f))$ and standard deviation σ .

TABLE I. Propagation Model and System Parameters

Parameter	value	
γ	25 dB [25]	
$\zeta(k)$	$k = 1$	-33 dB [21]
	$k = 2$	-43 dB [21]
	$k = 3$	-48 dB [21]
	$k \geq 4$	-50 dB [21]
δ	10 dB	
α	0.17 dB/m [22]	
A	1.4 dB [22]	
n_w	0.231 wall/m [26]	
L_w	5.9 dB [22]	
L_f	14.0 dB [22]	
σ	6.0 dB [24]	
η	-174 dBm/Hz	

III. FAIR RADIO RESOURCES DISTRIBUTION

In this section, the motivation for having a fair radio resource allocation mechanism in TVWS is shown, which is essentially the heterogeneity of the free TV channels. Moreover, frequency hopping as an enabler for such fairness is explained.

A. Heterogeneous Free Channels

Applying (5) to determine the maximum permissible AP transmission power at a specific location provides different values for different channels due to the following reasons. First - and most importantly - there are different adjacent channels indices; therefore, $\zeta(k)$ takes different values for different channels depending on which channels are used by the TV transmitter. Second, different used TV channels use different transmission powers, which provides different values of $S_L(x, y)$.

Not only is the AP transmission power different for different channels, but the TV transmission interference into different unoccupied channels also considerably varies. Measuring this interference in a specific area is a stand-alone contribution of this paper as explained in Section V. This PU interference originates from TV transmitter non-linearities in the form of spectral leakage and intermodulation products. Spectral leakage essentially affects the first adjacent channels while intermodulation products are found in different channels. Moreover, channels used by neighboring TV transmitters can also generate interference. Although TV transmission interference is more severe in outdoor operations, our measurements results presented in Section V show that the PU indoor interference into free TV channels is not negligible and considerably affects the performance of the SUs.

Having different permissible AP transmission power with different primary TV transmission interferences at different channels would result in having a wide range of throughput achieved when using different channels. The following subsection proposes frequency hopping as a solution to provide a fair distribution of the available channels among the APs.

B. Frequency Hopping

Frequency hopping is proposed in this paper to distribute the available heterogeneous free TV channels in a fair manner among the APs. By frequency hopping, it is meant that the APs

TABLE II. Equipments and measurements parameters

Equipment/Parameters	Type/Value
Antenna	R&S HE200 (RF Module 2)
Spectrum Analyzer	Anritsu MT8221B BTSMaster
Centre Frequency	666 MHz
Span	400 MHz
Resolution Bandwidth (RBW)	400 KHz
Preamplifier	On
Input Attenuation	0 dB
Detector	RMS
Sweptime (SWT)	840 ms

hop between the available channels in a random uncentralized manner. Through the use of frequency hopping, it is ensured that no APs will be holding all the time on the channels with a high SINR and none will be forced to use the low SINR channels during the entire time of operation. Therefore, by means of frequency hopping, all APs will eventually achieve similar long-term throughput. The achievable downlink throughput when transmitting on channel $k + L$ with the maximum permissible power is denoted as C_{k+L} and calculated as

$$C_{k+L} = \log_2 \left(1 + \frac{P_{k+L}^r(x, y)}{I_{k+L}^{SS} + I_{k+L}^{TV} + \eta} \right), \quad (8)$$

where I_{k+L}^{SS} is the interference from other APs occupying the same channel $k + L$, I_{k+L}^{TV} is the interference from the TV transmission into channel $k + L$ and η is the background noise.

Note that the throughput obtained using (8) and throughout the remainder of this paper is *per Hertz capacity* and given in [bits/sec/Hz]. For simplicity, the M available TV channels are locally re-indexed by the indices $1 \leq m \leq M$. Suppose that the SU terminal is served by its nearest AP that has an index i and hops among the M available channels with equal probabilities. Denote the channel used by the serving AP as \hat{m} at each hop. Thus, the average downlink throughput, C_{hop} , for each SU is calculated as

$$C_{hop} = \frac{1}{M} \sum_{m=1}^M \log_2 \left(1 + \frac{P_{k+L}^r(x, y)}{\sum_{\substack{j=0 \\ j \neq i}}^N (\beta_m P_{j,m}^r(x, y)) + I_m^{TV} + \eta} \right), \quad (9)$$

where

$$\beta_m = \begin{cases} 1 & \hat{m} = m \\ 0 & \text{Otherwise,} \end{cases}$$

Without loss of generality, one can neglect the interference of adjacent channels among the APs because the use case is a low-power short-range WiFi-like system.

IV. METHODOLOGY

The methodology for evaluating the proposed frequency hopping framework is explained in this section. A representative case study is considered in which data based on measurements and simulations are obtained. Moreover, a simulation of deployed APs performing frequency hopping in TVWS is performed based on the findings of the representative cases.

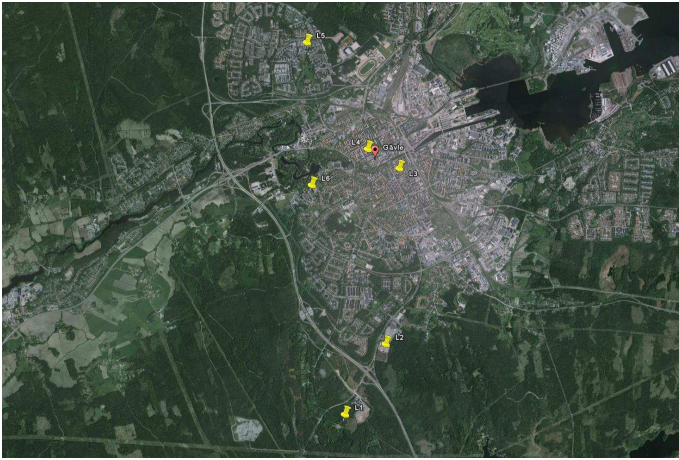


Figure 4. Measurements locations in Gävle. Measurements locations are the yellow markers

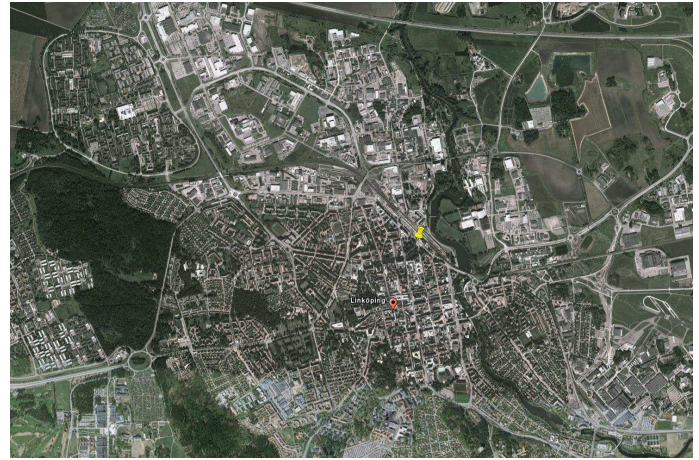


Figure 7. Measurements locations in Linköping. Measurements locations are the yellow markers.

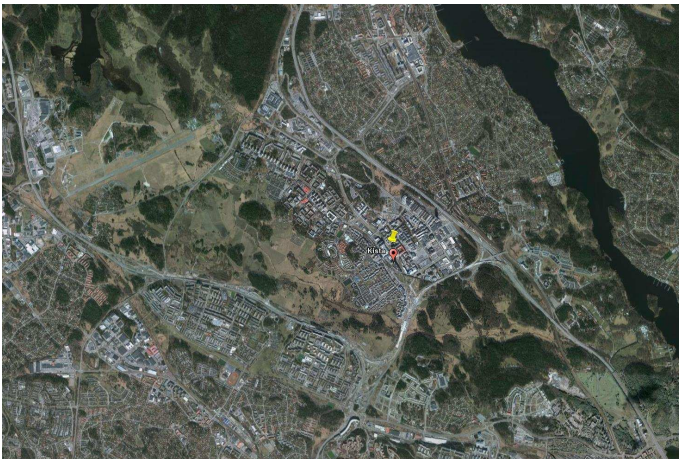


Figure 5. Measurements locations in Stockholm. Measurements locations are the yellow markers



Figure 8. Measurements setup

A. Obtaining TV Received Signal Power

SPLAT (RF signal propagation, loss, and terrain analysis tool) [27] is a simulation tool that is used to obtain the received signal power at each point inside the area under investigation. The input data to SPLAT are the transmitter properties (e.g., transmission power, mast height, and so forth) which were obtained from the Post and Transport Agency (PTS), the Swedish communication regulator. SPLAT uses the Longley-Rice propagation model [27] and terrain data that are available online at [27]. The simulation results for channel 24 in the surroundings of the Gävle area are shown as an example in Figure 11.

B. Measurements for Obtaining TV Interference into Free Channels

The TV transmission interference into free channels is not covered by the simulation model; rather, an empirical model for this interference is developed. Measurements are performed in three areas served by three different TV transmitters in Sweden, namely in the cities of Gävle, Stockholm and Linköping. In Gävle, the measurements were extensive

and performed in 6 different locations, marked as L1-L6. The measurements in Stockholm and Linköping are complementary and performed for comparisons and to consider areas with different characteristics. Table III shows the GPS coordinates and descriptions of the measurements locations. Google Maps images for the measurements locations are also presented in Figures 4, 5, and 7.

The measurements are performed using a set up that consists of an antenna, a spectrum analyzer and a PC. The antenna and the spectrum analyzer are used to capture the signal in the entire TV band, which is then recorded using the PC for further analysis. The PC also controls the spectrum analyzer. Figure 8 presents a field photo of the measurements setup. Moreover, the equipments and other parameters are provided in Table I.

V. RESULTS

The results can be divided into three parts, namely, fetching the interference from the TV transmission into the free channels, obtaining the model parameters part and evaluation

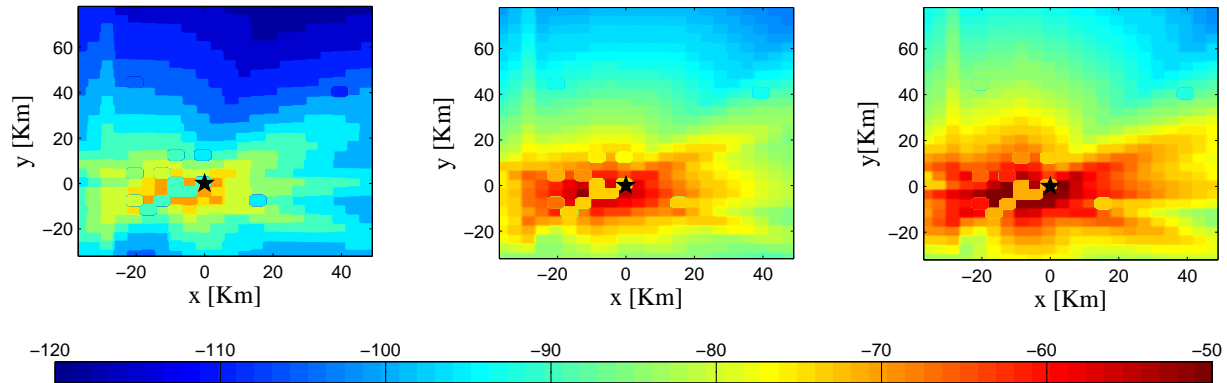


Figure 6. Maximum allowed transmission power density [dBm/Hz] for a SU in channels 25, 48, and 35 (from left to right). All the color-coded values correspond to the Gävle area.

TABLE III. Measurements Locations

Measurements Location	Description	GPS coordinates	Active TV channels	
Gävle	L1	Next to the TV transmitter antenna	60.6400 N, 17.1322 E	
	L2	In a supermarket	60.6417 N, 17.1428 E	
	L3	In the city center	60.6734 N, 17.1395 E	24, 27, 30, 32, 46, 50
	L4	In a school	60.6689 N, 17.1514 E	
	L5	In an apartment	60.6904 N, 17.1198 E	
	L6	At University of Gävle	60.6692 N, 17.1210 E	
Stockholm	Office complex (ELECTRUM)	59.4053 N, 17.9489 E	21, 27, 31, 39, 40, 42, 53	
Linköping	Central train station	58.4166 N, 15.6250 E	23, 36, 39, 42, 50, 53, 55, 56	

of the deployed APs part. The AP evaluation is based on the achieved throughput.

A. Interference from TV Transmission into Free Channels

The interference from the TV transmission is caused by the non-linearities introduced by the TV transmitter power amplifier. These non-linearities are divided into spectrum leakage and intermodulation products. Figure 9 is a qualitative illustration of the measured leaked power at location L2 in Gävle as an example. In Figure 10, the intermodulation products are shown. For later analysis the quantitative findings of both the spectrum leakage and the intermodulation products are used.

To reflect the extent of the variety of the free TV channels, let us define $\gamma_0(k+L)$ as the ratio between the permissible SU transmission in channel $k+L$ and the TV interference into the same channel. In many channels, the value of γ_0 approaches ∞ as the best case, while as the worst case in the measurements locations, the value of $\gamma(47)$ is equivalent to 26 dB in location L5.

B. Obtaining Model Parameters

As described in Subsection IV, the received TV signal power and the TV interference into free channels are needed. The received TV signal power is obtained by SPLAT, as shown in Figure 11 as an example of one channel.

Using the received TV signal power at all points in the study area, the maximum permissible transmission power is

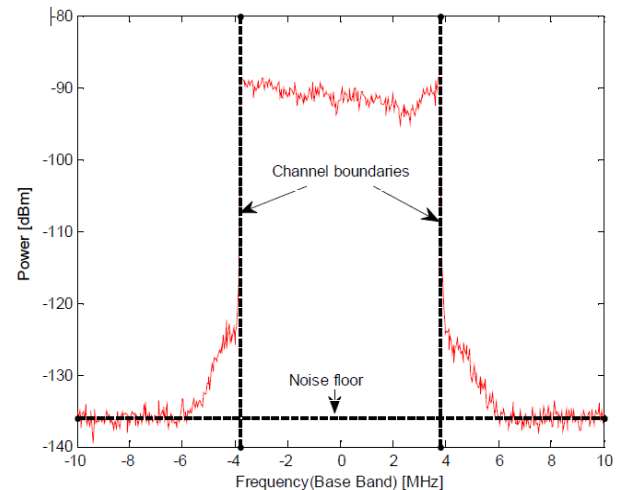


Figure 9. Measured spectrum of channel 30 at location L2 in Gävle. The leaked power from channel 30 into its adjacent channels is observed.

calculated using (5). Figure 6 shows this permissible transmission power density for channels 25, 48, and 35 in the Gävle area. These three channels have been chosen as representatives for the 1st, 2nd and 3rd adjacent channels, respectively. The figure shows how the permissible transmission power for SU differs in different channels and different locations. For example, SUs can transmitting in channel 35 with an approximately 20 dBm/Hz higher power density compared to transmit in

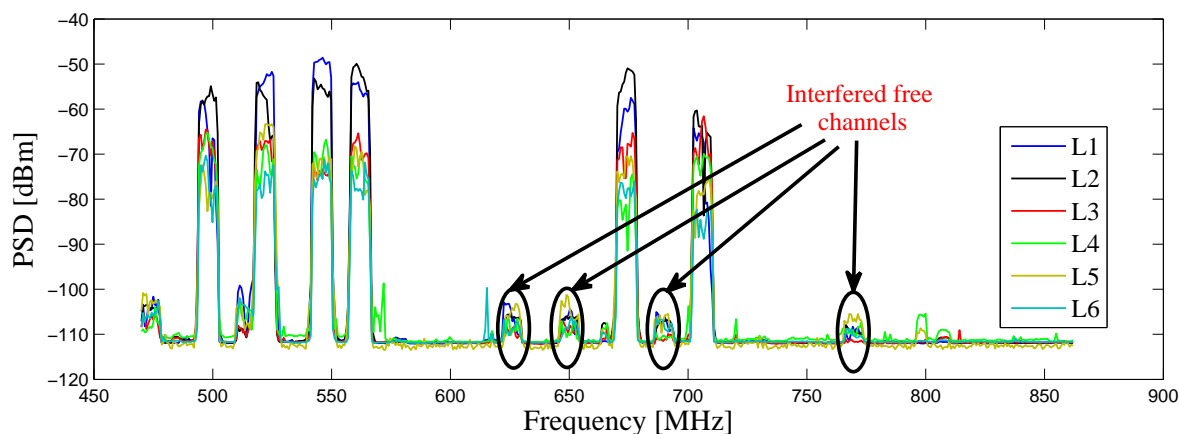


Figure 10. Spectrum occupancy for the entire TV band in the measurements locations in Gävle, L1-L6.



Figure 11. SPLAT results for the received signal power for channel 24 [dBm] in the Gävle area as a function of the TV receiver location.

channel 25.

C. APs Throughput

At first, to show the creditability of using the frequency hopping scheme, the achieved throughput without and with hopping is studied. Assume an AP serving area of 100 m^2 and three APs using three different TVWS channels without hopping. AP1 uses channel 47, AP2 transmits on channel 34, and AP3 operates on channel 36. These three channels are selected to have three different classes of the provided throughput. Figure 12 shows the cumulative distribution function (CDF) of the throughput on each channel when each AP holds on its channel. As shown in this figure, user 1 served by AP1 obtains the lowest throughput all the time with an average of 2.6 bits/sec/Hz, while user 3 served by AP3 achieves the highest throughput with an average of 6.4 bits/sec/Hz. Applying frequency hopping among the three channels for all APs would then make the three users achieve the same

throughput with an average of 5.8 bits/sec/Hz. Therefore, the three available channels are shared among the three APs in a fair manner.

As another case, Figure 16 shows the achievable throughput per square meter in Stockholm when using different numbers of APs for different floor areas. All the findings shown in Figure 16 consider a hopping set of 3 channels, which are channels 24, 36, and 48 chosen randomly.

Now, suppose that frequency hopping is applied among a certain set of channels, called a hopping set; then the achieved throughput depends on the permissible transmission power and the TV interference on this hopping set. As an example, consider the following three cases. In Case 1, the hopping set is three interfered channels with low permissible transmission power; for this case, use channels 44, 45, and 47. Case 2 uses better channels than Case 1, namely channels 25, 34 and 35. the case 3 hopping set is the best, where chan-

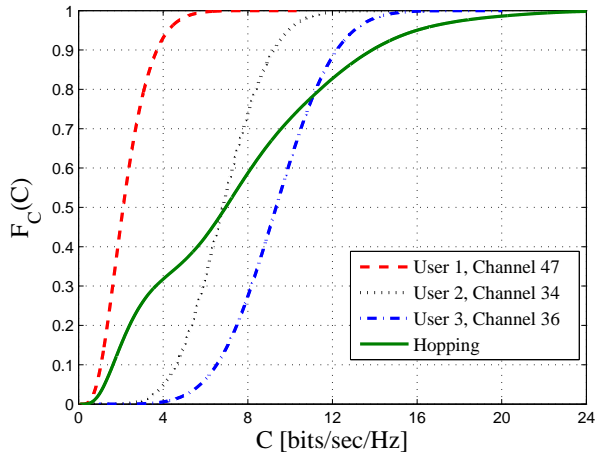


Figure 12. Achieved throughput CDF when using three different channels individually and when hopping is applied.

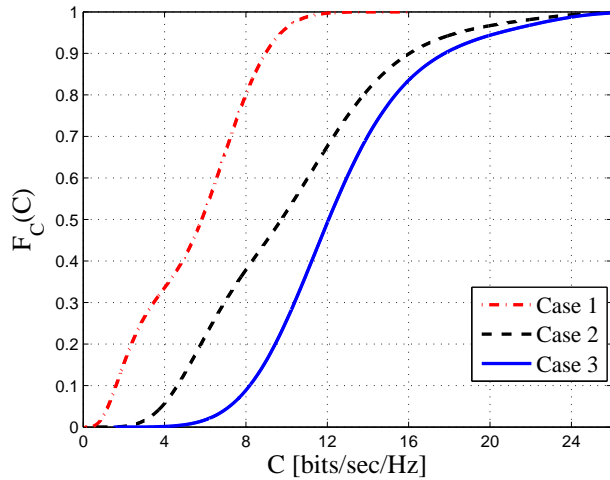


Figure 13. Achieved throughput CDF for three different cases when 3 channels are used by the APs with frequency hopping.

nels 35, 36, and 51 are used. As Figure 13 depicts, hopping among the case 1 set provides the lowest throughput, while using the channels in case 3 as a hopping set provides the highest throughput. the throughput in case 2 is in between that of cases 1 and 3. Quantitatively, the case 1 set provides approximately 50% of the throughput that the case 3 set achieves.

An important factor for the achieved throughput is the size of the hopping set (i.e., the number of channels). In this regard, a simulation is conducted in which the set size is changed. The hopping set is chosen such that the average channel quality is preserved when comparing different set sizes. Figure 14 shows that the achieved throughput changes almost linearly when increasing the hopping set from 1 to 4 channels in all regions of the CDF curve. However, for the mean and above the 50 percentile, when increasing the hopping size beyond 4 channels, the linear increase stops and the gain in the throughput tends to saturate. This result is due to the fact that APs using the same channel are more likely to be further

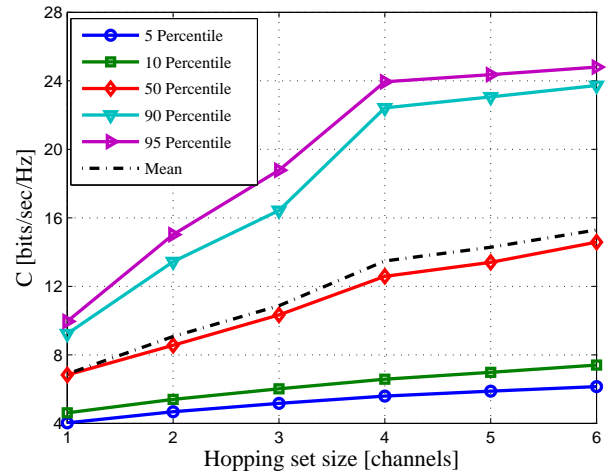


Figure 14. The 5, 10, 50, 90 and 95 percentile for the achieved throughput when using different sizes of hopping sets.

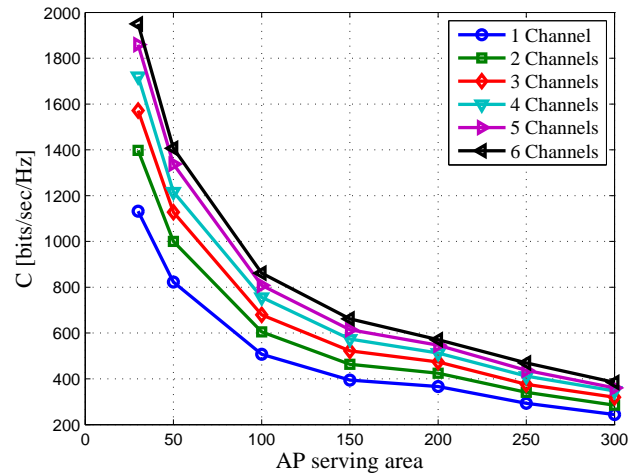


Figure 15. Overall throughput achieved in the building located in Gävle, L4 using different AP serving areas (i.e., different numbers of APs).

separated when higher hopping sets are used.

Together with the hopping set, the AP serving area, which determines the number of APs in the building, determines the achieved throughput in the entire building. Figure 15 shows how the total throughput provided by the WiFi-like system is affected by changes in the AP serving area and the hopping set. Figure 15 shows that increasing the AP serving area decreases the provided throughput for the entire building because there are less resources to handle the traffic. However, increasing the AP serving area increases the distances between the APs using the same channel while hopping, which in turn decreases the interference among the APs. Therefore, the decrease in the throughput does not occur linearly with the increase in the AP serving area. It is important to study the throughput map in the building. Figure 17 presents a color-coded map of the throughput in one of the building floors with the APs locations. The figure is generated considering a deployment of 25 APs. In general, it is observed from the figure that the closer to the

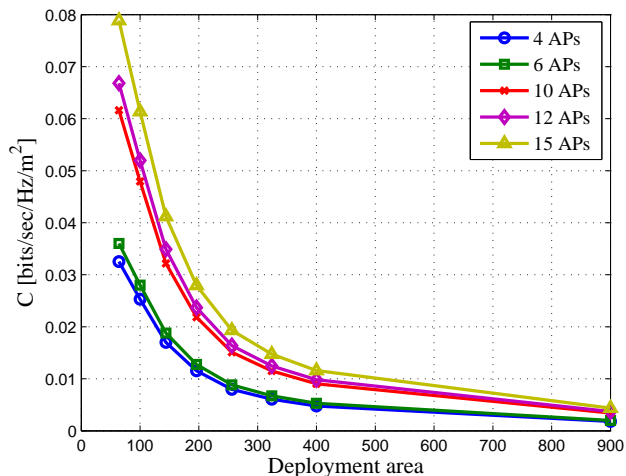


Figure 16. Achievable capacity density in the simulated building located in Stockholm in the measurements location using different numbers of APs and different floor areas.

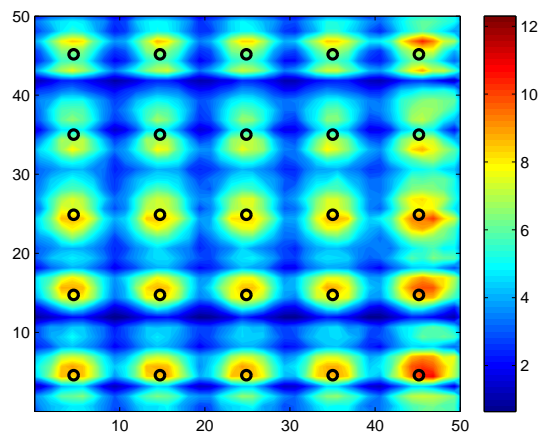


Figure 17. Average throughput at different points in one of the building's floors located in Gävle. The black rings are the deployed APs.

AP that the user is, the higher the throughput that they receive. This result is not only because of the higher received power from the AP but also because of being further from the other APs that use the same channel and hence, less interference is experienced. Moreover, the APs located closer to the edges of the building supply higher throughput because other interfering APs are located at one side and therefore have longer distances to APs located at the edges. On the other hand, the APs in the middle receive interference from all directions with longer distances from the interferers, which decreases their provided throughput.

For comparison, Figure 18 shows the upper and lower bounds for the entire building throughput for the simulated office building located in Gävle, Stockholm and Linköping. The bounds are considered when the hopping set is composed of 3 channels. For the upper bounds, the best 3 channels in each location are used for the hopping set, while the worst 3 channels are used to reach the lower throughputs'

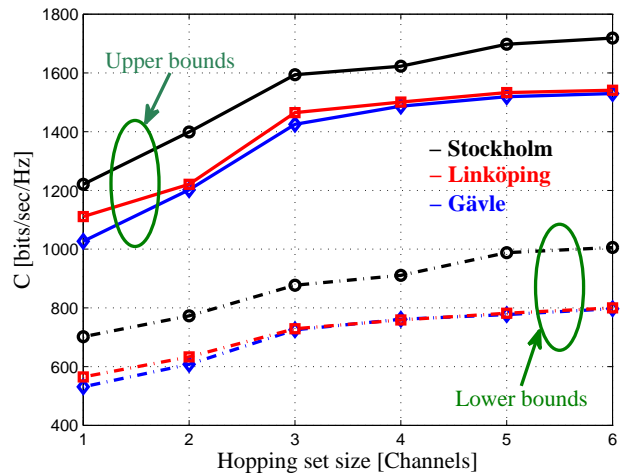


Figure 18. Throughput's upper and lower bounds in the measurements locations in Gävle, Stockholm and Linköping.

bounds. As shown in the figure, in the Stockholm area, higher throughputs are attainable in both sides due to the existence of higher buildings and more objects that attenuate more of the interfering signals. An important observation here is that the TV signal in Stockholm is still high compared to that in Gävle and Linköping, which enables high secondary transmission power. This high received TV signal is observed despite the high building and existence of attenuating objects, which is due to some consideration in the system design of the TV mast height and the transmission power. Comparing Gävle and Linköping, it is observed that the performance is nearly identical with slightly higher performance in Linköping. Note that these results are for the measurements locations which are specific cases. However, the general tendency can be extrapolated.

VI. CONCLUSION

Throughout this paper, the performance of a WiFi-like secondary network deployed in an office environment has been studied. Three different locations in three different cities, namely Gävle, Stockholm and Linköping, all located in Sweden, are considered for the studies within this paper. The secondary WiFi-like network operates in a TVWS using the geo-location database spectrum opportunities framework. The main metric used in the performance evaluation is the achievable downlink throughput for the access points. This achievable throughput is determined using the permissible transmission power, which protects the TV reception, the interference among the access points and the TV transmission interference. All these parameters have been obtained using either measurements or simulations for a realistic scenario. The results have shown that different TV channels experience a large variety in their provided throughput. Therefore, frequency hopping is applied for fair resource distribution among the access points. Moreover, an investigation on the impacts of the size of the hopping set and the number of deployed APs has also been conducted.

REFERENCES

- [1] M. Hamid and N. Björnsell, "Frequency hopping for fair radio resources allocation in TVWS," in 11th Int. Conf. Wireless and Mobile Commun. (ICWMC), Oct. 2015, pp. 71–76.

- [2] M. Dohler, R. W. Heath, A. Lozano, C. B. Papadias, and R. A. Valenzuela, "Is the phy layer dead?" *IEEE Communications Magazine*, vol. 49, no. 4, Apr. 2011, pp. 159–165.
- [3] V. Chandrasekhar, J. G. Andrews, and A. Gatherer, "Femtocell networks: a survey," *IEEE Communications Magazine*, vol. 46, no. 9, Sep. 2008, pp. 59–67.
- [4] G. Staple and K. Werbach, "The end of spectrum scarcity [spectrum allocation and utilization]," *IEEE Spectrum*, vol. 41, no. 3, Mar. 2004, pp. 48–52.
- [5] M. Wellens, J. Wu, and P. Mahonen, "Evaluation of spectrum occupancy in indoor and outdoor scenario in the context of cognitive radio," in *2nd International Conference on Cognitive Radio Oriented Wireless Networks and Communications*, (CrownCom), Aug. 2007, pp. 420 – 427.
- [6] R. I. C. Chiang, G. B. Rowe, and K. W. Sowerby, "A quantitative analysis of spectral occupancy measurements for cognitive radio," in *Vehicular Technology Conference, 2007. VTC2007-Spring*. IEEE 65th, Apr. 2007, pp. 3016–3020.
- [7] T. M. Taher, R. B. Bacchus, K. J. Zdunek, and D. A. Roberson, "Long-term spectral occupancy findings in chicago," in *IEEE Symposium on New Frontiers in Dynamic Spectrum Access Networks (DySPAN)*, May 2011, pp. 100–107.
- [8] J. Mitola, "Cognitive radio for flexible mobile multimedia communications," in *IEEE Int. Workshop on Mobile Multimedia Commun.(MoMuC)*, 1999, pp. 3 –10.
- [9] S. Haykin, "Cognitive radio: brain-empowered wireless communications," *IEEE Journal on Selected Areas in Communications*, vol. 23, no. 2, February 2005, pp. 201 – 220.
- [10] S. Stotas and A. Nallanathan, "Enhancing the capacity of spectrum sharing cognitive radio networks," *IEEE Transactions on Vehicular Technology*, vol. 60, no. 8, Oct. 2011, pp. 3768–3779.
- [11] —, "On the throughput and spectrum sensing enhancement of opportunistic spectrum access cognitive radio networks," *IEEE Transactions on Wireless Communications*, vol. 11, no. 1, Jan. 2012, pp. 97–107.
- [12] A. Attar, O. Holland, M. R. Nakhai, and A. H. Aghvami, "Interference-limited resource allocation for cognitive radio in orthogonal frequency-division multiplexing networks," *IET Communications*, vol. 2, no. 6, Jul. 2008, pp. 806–814.
- [13] G. Hattab and M. Ibnkahla, "Multiband spectrum access: Great promises for future cognitive radio networks," *Proceedings of the IEEE*, vol. 102, no. 3, Mar. 2014, pp. 282–306.
- [14] A. Ghasemi and E. Sousa, "Spectrum sensing in cognitive radio networks: requirements, challenges and design trade-offs," *IEEE Communications Magazine*, vol. 46, no. 4, April 2008, pp. 32 –39.
- [15] M. Denkovska, P. Latkoski, and L. Gavrilovska, "Geolocation database approach for secondary spectrum usage of TVWS," in *19th Telecommun. Forum (TELFOR)*, Nov. 2011, pp. 369 –372.
- [16] M. Nekovee, T. Irnich, and J. Karlsson, "Worldwide trends in regulation of secondary access to white spaces using cognitive radio," *IEEE Wireless Communications*, vol. 19, no. 4, Aug. 2012, pp. 32–40.
- [17] E. Obregon and J. Zander, "Short range white space utilization in broadcast systems for indoor environments," in *IEEE Symp. on New Frontiers in Dynamic Spectrum Access Networks (DySPAN)*, Apr. 2010, pp. 1–6.
- [18] L. Simic, M. Petrova, and P. Mahonen, "Wi-Fi, but not on steroids: Performance analysis of a Wi-Fi-like network operating in TVWS under realistic conditions," in *IEEE Int. Conf. on Commun. (ICC)*, Jun. 2012, pp. 1533–1538.
- [19] Y. Yang, L. Shi, and J. Zander, "On the capacity of Wi-Fi system in TV white space with aggregate interference constraint," in *8th Int. Conf. on Cognitive Radio Oriented Wireless Networks (CROWNCOM)*, Jul. 2013, pp. 123–128.
- [20] "Model integration and spectrum assessment methodology, QUASAR Deliverable D5.1," *Tech. Rep.*, Mar. 2011.
- [21] E. Obregon, L. Shi, J. Ferrer, and J. Zander, "Experimental verification of indoorTV white space opportunity prediction model," in *Proceedings of the Fifth International Conference on Cognitive Radio Oriented Wireless Networks Communications (CROWNCOM)*, Jun. 2010, pp. 1–5.
- [22] W. Yamada, M. Sasaki, T. Sugiyama, O. Holland, S. Ping, B. Yeboah-Akokuah, J. Hwang, and H. Aghvami, "Indoor propagation model for TV white space," in *2014 9th International Conference on Cognitive Radio Oriented Wireless Networks and Communications (CROWNCOM)*, Jun. 2014, pp. 209–214.
- [23] "Digital mobile radio: COST 231 view on the evolution towards 3rdgeneration systems," *Commission of the European Communities, Tech. Rep.*, 1989.
- [24] "Propagation data and prediction method for the planning of indoor radio communication systems and radio local area networks in the frequency range 900 MHz to 100 GHz, ITU-R P.1238-7," *Tech. Rep.*, 2012.
- [25] A. Sahai, M. Mishra, R. Tandra, K. Woyach, G. Atia, and V. Saligrama, "Prospects and challenges for spectrum sharing by cognitive radios," in *EE Seminar at Harvard*, Feb. 2009.
- [26] D. H. Kang, K. W. Sung, and J. Zander, "Attainable user throughput by dense Wi-Fi deployment at 5 GHz," in *IEEE 24th Int. Symp. on Personal Indoor and Mobile Radio Commun. (PIMRC)*, Sep. 2013, pp. 3418–3422.
- [27] SPLAT! [Online]. Available: <http://www.qsl.net/kd2bd/splat.html>[retrieved:Aug.,2015]



www.iariajournals.org

International Journal On Advances in Intelligent Systems

🔗 issn: 1942-2679

International Journal On Advances in Internet Technology

🔗 issn: 1942-2652

International Journal On Advances in Life Sciences

🔗 issn: 1942-2660

International Journal On Advances in Networks and Services

🔗 issn: 1942-2644

International Journal On Advances in Security

🔗 issn: 1942-2636

International Journal On Advances in Software

🔗 issn: 1942-2628

International Journal On Advances in Systems and Measurements

🔗 issn: 1942-261x

International Journal On Advances in Telecommunications

🔗 issn: 1942-2601